Adv. Space Res. Vol.5, No.11, pp.117-171, 1985 0273-1177/85 $0.00 + .50

CHAPTER IV

MODELS OF VENUS NEUTRAL UPPER ATMOSPHERE: STRUCTURE AND COMPOSITION

G. M. Keating,[1] J. L. Bertaux,[2] S. W. Bougher,[3]
T. E. Cravens,[4] R. E. Dickinson,[3] A. E. Hedin,[5]
V. A. Krasnopolsky,[6] A. F. Nagy,[4] J. Y. Nicholson III,[7]
L. J. Paxton[8] and U. von Zahn[9]

[1] *NASA, Langley Research Center, Hampton, VA, U.S.A.*
[2] *Service d'Aéronomie du CNRS, Verrieres le Buisson, France*
[3] *National Center for Atmospheric Research, Boulder, CO, U.S.A.*
[4] *University of Michigan, Ann Arbor, MI, U.S.A.*
[5] *NASA, Goddard Space Flight Center, Greenbelt, MD, U.S.A.*
[6] *Space Research Institute, U.S.S.R. Academy of Sciences, Moscow 117810, U.S.S.R.*
[7] *Systems and Applied Sciences Corp., Hampton, VA, U.S.A.*
[8] *Naval Research Laboratory, Washington, DC, U.S.A.*
[9] *Physikalisches Institut, Universität Bonn, 5300 Bonn 1, F.R.G.*

ABSTRACT

Models of the Venus neutral upper atmosphere, based on both in-situ and remote sensing measurements, are provided for the height interval from 100 to 3,500 km. The general approach in model formulation was to divide the atmosphere into three regions: 100 to 150 km, 150 to 250 km, and 250 to 3,500 km. Boundary conditions at 150 km are consistent with both drag and mass spectrometer measurements. A paramount consideration was to keep the models simple enough to be used conveniently. Available observations are reviewed. Tables are provided for density, temperature, composition (CO_2, O, CO, He, N, N_2, and H), derived quantities, and day-to-day variability as a function of solar zenith angle on the day- and nightsides.

Estimates are made of other species, including O_2 and D. Other tables provide corrections for solar activity effects on temperature, composition, and density. For the exosphere, information is provided on the vertical distribution of normal thermal components (H, O, C, and He) as well as the hot components (H, N, C, O) on the day- and nightsides.

1. Introduction

Major advances in our knowledge of the Venus neutral upper atmosphere have occurred over the last 14 years. Early reference

atmospheres (Noll and McElroy, 1972) gave exospheric temperatures of 700 K, indicated atomic oxygen was a relatively minor species in the thermosphere, and estimated large solar activity variations. Now we know that exospheric temperatures range from 100 to 300 K, atomic oxygen is a major species in the thermosphere, and solar activity variations are quite small.

New reference models are provided here for the neutral atmosphere from 100 to 3,500 km, reflecting these and many other new results. Most of the data used to formulate these models come from measurements obtained from the Pioneer and Venera 11 and 12 spacecraft, all of which arrived at Venus in December 1978. Results from these missions concerning the upper atmosphere are reviewed in great detail in various chapters of the book entitled Venus (see von Zahn et al., 1983; Seiff, 1983a; Krasnopolsky, 1983; Krasnopolsky and Parshev, 1983; Taylor et al., 1983; Schubert, 1983). The most recent results are described in Advances in Space Research, Volume 5, Number 9 (1985). See also Moroz (1981b). Prior to 1979, measurements of the neutral upper atmosphere were limited to remote sensing from the Earth and from the Mariner and earlier Venera spacecraft. These earlier results were reviewed, for example, in Space Science Reviews, Volume 20, Numbers 3 and 4, 1977, and by Kuzmin and Marov (1974).

The spacecraft data used in formulating these proposed reference models are based on the 17 experiments listed in Table 4-1. For brevity, the experiments will be referred to by the acronyms in the table.

The general approach in model formulation was to divide the upper atmosphere into three regions: 100 to 150 km, 150 to 250 km, and 250 to 3,500 km. Evaluation was first made of the region from 150 to 250 km, where the most extensive measurements have been obtained. Then the upper and lower limits of this model were used as boundary conditions for the adjacent regions. A paramount consideration was to keep the models simple enough to be used conveniently. For the region between 150 and 250 km, the vertical distribution of density, temperature, composition (including H) and various derived quantities are tabulated for noon and midnight conditions. The vertical distribution of density, temperature, and composition are also tabulated for intermediate solar zenith angles.

The solar activity variations at 150 km in composition and temperature are provided in a form making it convenient to calculate the estimated variations at other altitudes. Thus, the conditions as a function of altitude for any latitude, local solar time, and solar activity level can be rapidly estimated. The characteristic day-to-day variability of the atmosphere on the dayside and nightside is also provided. In the region between 150 and 250 km, the models are based principally on complementary in-situ mass spectrometer and drag measurements.

From 100 to 150 km, the day and night conditions are tabulated for density, temperature, composition, and various derived quantities. In this region, the data are very sparse and conditions are much more uncertain than above 150 km so that the models are more dependent on theory and extrapolation. Thus, even though the conditions in this region essentially control conditions at higher altitudes, much less about them is actually known.

Above 250 km, the composition, species scale heights, and total density are provided for the dayside and nightside. The models are based on both in-situ and remote sensing measurements. The normal thermal components of H, O, C, and He, as well as the hot components of H, N, C, and O are included.

First, the 150-250 km models are discussed, followed by the 100 to 150 km models, and finally, the neutral atmosphere models for altitudes above 250 km.

2. Models Between 150 km and 250 km

2.1 Measurements

In-situ measurements and derived quantities were obtained in the 150- to 250-km regime by means of the Pioneer Venus BNMS [He, N_2, CO, CO_2, K_z, T, P, ρ] (von Zahn et al., 1980), ONMS [He, N_2, N, CO, CO_2, O, T, ρ, P, K_z] (Niemann et al. 1980), and OAD [ρ, H_ρ, T, O, CO_2, P] (Keating et al., 1980) experiments.

From complementary measurements of the Pioneer Venus OIMS, atomic hydrogen (Brinton et al., 1980) atomic carbon (Fox, 1982) and deuterium (Hartle and Taylor, 1983; Kumar and Taylor,

1985) are determined. Remote measurements of H and He were obtained from Veneras 11 and 12 (Bertaux et al., 1981 and 1985). From the Pioneer Venus OUVS experiment, concentrations of thermal atomic oxygen (Paxton and Meier, 1985), atomic hydrogen (Paxton et al, 1985), and atomic carbon (Paxton, 1983) were derived.

2.2 Model Formulation

The data from the Pioneer Venus ONMS and OAD experiments were combined, taking into account the unique advantages of each experiment. The ONMS could identify the detailed compositional variations while the OAD experiment could obtain in a straightforward manner total density and density scale heights, and was not subject to short- or long-term drifts in sensitivity. The concentration n_i, of species i at 150 km can be given by

$$n_i = k\, n_i' \qquad (1)$$

where n_i' = number density measured by ONMS before the sensitivity correction (1.63) given in the Hedin et al. (1983) model is applied, and k = sensitivity correction to ONMS. Values of k for CO_2 and O, one of which always provides the major drag effect at these altitudes, were chosen to be consistent with the OAD drag measurements. This choice was prompted by indications that the values of k for CO_2 and O were different (von Zahn et al., 1980; Massie et al., 1983). There were also indications that the k of CO and N_2 were different (Massie et al., 1983), but this could not be easily checked with drag data since both species have the same molecular weight. Thus, it was assumed that the values of k for the other species were equal to the value for O. In addition to solving for the values of k, the mean temperature and the diurnal and solar activity variations of temperature were determined simultaneously from the OAD vertical structure measurements, assuming the ONMS mixing ratios at 150 km corrected for k. A comparison between the resulting reference model and the OAD data is shown in Figure 4-1. The OAD data were obtained within a half hour of each of the indicated times: midnight and noon. The model curves are consistent with the average solar activity level and latitude of the two sets of data points. The resulting coefficients, consistent with the formulation of Hedin et al. (1983), are shown in Table 4-2. As may be recognized, the CO_2 sensi-

tivity (1.83 ± 0.06) is higher than that of O (1.58 ± 0.03). The higher value of k for CO_2 indicates a somewhat warmer thermosphere below 150 km than estimated by Hedin et al. (1983) in order for drag data above 150 km to be consistent with values near 115 km obtained from entry probes.

Shown in Table 4-3 is a comparison of this VIRA model with calculated concentrations of species obtained near 150 km through other empirical or theoretical studies. Although the agreement is generally good, in some cases, there is substantial disagreement (for example Bertaux et al., 1985). The difference, by a factor of 2, between helium amounts measured by the mass spectrometric and airglow techniques is typical also from the Earth's atmosphere (Anderson et al., 1979). Helium concentrations provided in these models are based on mass spectrometer measurements.

Above 150 km, it is assumed that diffusive equilibrium is established and each species distributes itself independently according to its molecular weight. This allows the solution to be independent of any assumed diurnal variation of K(z), the eddy diffusion coefficient. Thus,

$$n_{i,1} = n_{i,o} \left(\frac{T_o}{T_1}\right)^{1+\alpha} \exp\left[- \int_{Z_o}^{Z_1} \frac{g(z) m_i}{R^* \; T(z)} \, dz \right] \qquad (2)$$

where subscript o indicates a different height than subscript 1;

T = ambient temperature, K;

m_i = molecular weight of i^{th} constituent, g;

R^* = 8.3134×10^7, erg K^{-1} $mole^{-1}$;

$g(z) = g_o (1 + z/R)^{-2}$; g_o = 886.945 cm/s^2; R = 6052 km; and

α = thermal diffusion coefficient
(-0.4 for helium, -0.25 for H, O for other species).

Following Keating et al., (1980), the assumed form of the temperatu profiles are:

when $T_\infty \geq T_{115}$,

$$T_{(z)} = T_\infty - (T_\infty - T_{z_I}) \exp [-s (z - z_I)] \qquad z \leq z_I \quad (3)$$

$$T_{(z)} = T_L - (T_L - T_{z_I}) \exp [s (z - z_I)] \quad (4)$$

$$z_I \geq z \geq 115 \text{ km}$$

$$T_{z_I} = \frac{1}{2} (T_L + T_\infty) \quad (5)$$

$$T_L = \frac{T_{115} - \frac{1}{2} T_\infty \exp [s (115 - z_I)]}{1 - \frac{1}{2} \exp [s (115 - z_I)]} \quad (6)$$

where T_{115} = temperature at 115 km

T_∞ = exospheric temperature

s = constant taken as 0.069 when $T_\infty \geq T_{115}$ and taken as 0.2 when $T_\infty < T_{115}$

z_I = inflection altitude taken as 143.9 km when $T_\infty \geq T_{115}$ and taken as 115 km when $T_\infty < T_{115}$

when $T_\infty < T_{115}$

$$T_{(z)} = T_\infty - (T - T_{115}) \exp [-s (z - 115)] \quad z \geq 115 \quad (7)$$

The resulting expressions for $n_{i(z)}$ have closed-form solutions.

The boundary conditions at lower altitudes of temperature and density were essentially consistent with accelerometer measurements from the Pioneer Venus multiprobes (Seiff, 1983c) and with OIR temperatures (Schofield and Taylor, 1983a).

Using this general approach the vertical structure of CO_2, O, CO, N_2, N, He, C, N, H, as well as ρ, T, and P was formulated

from 150 to 250 km. The values of H are based on the results of Brinton et al. (1980) derived from OIMS and ONMS measurements. (See Figure 4-2.) Bertaux et al. (1982) recommended that the Brinton et al. (1980) values of H be increased by 1.2 times the k value for the drag-determined O sensitivity. We thus increased the H concentrations given here by a factor of (1.2) · (1.57) = 1.9. The large diurnal variation of H with its predawn bulge has now been traced over three diurnal cycles as shown in Figure 4-3 (Taylor, Jr. et al., 1985). An independent determination of H from OUVS Lα data gives results consistent with Brinton et al., 1980 (see Figure 4-4).

Values of atomic carbon estimated by Fox (1982) are given in Figure 4-5 for two assumed O_2/CO_2 ratios based on Pioneer Venus observations of CO, CO^+, C^+, and other species and the large atomic carbon dayglow intensities measured by Mariner 10 (Broadfoot et al., 1974). From a detailed analysis of atomic carbon from OUVS observations, Paxton (1983, 1985a) concludes that an O_2 to CO_2 mixing ratio of 0.3% yielded the best agreement with theory for both the 156- and 166-nm data sets. Accordingly, we have chosen the left curve of Figure 4-5 as the reference atomic carbon profile for the dayside. The low O_2 to CO_2 ratio is in fair accord with Krasnopolsky (1982) and Krasnopolsky and Parshev (1983).

Deuterium concentrations have been deduced from OIMS measurements of the mass-2 ion (McElroy et al., 1982; Hartle and Taylor, 1983; Kumar and Taylor, 1985). Recent calculations by Kumar and Taylor (1985) from OIMS observations give the D/H ratio near the homopause (~130 km) in the predawn region as ~2% (1.4% to 2.5%).

2.3 Noon and Midnight Models

Models were generated for the approximate intermediate solar activity conditions during the entry of the Pioneer Venus multiprobes and the Venera 11 and 12 probes, for an $\bar{F}_{10}$ of 150. ($\bar{F}_{10}$ is defined here as the 81-day average of 10.7 cm solar flux at one astronomical unit divided by 10^{-22} Wm^{-2} Hz^{-1}).

The model latitude chosen was 16°N, consistent with the latitude of the Pioneer Venus Orbiter periapsis during this initial

period. For comparison, the tabulations in Hedin et al. 1983 are for the equator and $\bar{F}_{10}$ = 200. Shown in Figure 4-6 is the resulting noon reference model for $\bar{F}_{10}$ = 150 at latitude 16°N. The exospheric temperature is given as 284 K. It may be observed that atomic oxygen is the principal species over most of the altitude range. Shown in Figure 4-7 is the corresponding midnight reference model with $\bar{F}_{10}$ = 150 and latitude = 16°N. The temperature decreases only slightly with increasing altitude from 150 to 250 km. The exospheric temperature is given as 127 K. With such a low temperature, the heavier species decrease rapidly with altitude, leaving hydrogen and helium as the major species above 200 km. The corresponding tabulations of noon (dayside) and midnight (nightside) conditions are shown in Table 4-4 and 4-5 respectively. The altitude, density, temperature, composition, and mean molecular weight are shown. Tabulations of derived quantities for noon and midnight conditions are provided in Tables 4-6 and 4-7 respectively. The expressions for the derived quantities are consistent with those in the U.S. Standard Atmospheres, 1976. The derived quantities from left to right are the following: total number density (NTOT) (cm^{-3}), pressure (P) (mb), speed of sound (SS) ($cm\ s^{-1}$), mean free path (MFP) (cm), pressure scale height (HP) (km) and density scale height (HRHO) (km).

2.4 Variations With Solar Zenith Angle

Large variations with local solar time and solar zenith angle in the density and temperature have been detected by the OAD (Keating et al., 1979a, 1979b, and 1980) and ONMS (Niemann et al., 1979b and 1980) experiments. These variations were much different from earlier predictions. Shown in Figure 4-8 is the observed variation of density measured at 160 km by OAD (Keating et al., 1980) and the corresponding predicted density variation (combining O, CO, and CO_2) indicated by the early Dickinson and Ridley theoretical model (Dickinson and Ridley, 1977). On the other hand, solar zenith angle appears to be the most important variable, as predicted by Dickinson and Ridley (1977). Ordering data with respect to solar zenith angle results in some problems due to some observed asymmetries with respect to local solar time. But for the purpose of providing simple useful models, the advantages outweigh the disadvantages.

The strongest asymmetries with respect to local solar time occur for the lightest species, H (See Figures 4-2, 4-3, and 4-4) and He (Niemann et al., 1980). Figure 4-9 shows the diurnal variations of helium at 170 km over 3 diurnal cycles of ONMS data (a, b, c) (reviewed by von Zahn et al., 1983). Both H and He maximize in the predawn region near where temperatures minimize. These asymmetries may be caused by a combination of day-to-night flow and superrotation of the upper atmosphere of Venus (rotation in same sense, but more rapid than the planet) (Mayr et al., 1980 and 1985). Thus, the dynamics causing the night-side helium bulge on Venus are apparently analogous to those causing the winter helium bulge on Earth (Keating and Prior, 1968).

For the purposes of estimating conditions at any latitude and local solar time on the planet, the average density, temperature, and composition were determined as a function of solar zenith angle. Since the solar declination remains ~0° for Venus, the relation between solar zenith angle (SZA), local solar time (LST), and latitude (LAT) may be approximated by

$$\cos(\mathrm{SZA}) = \cos(\mathrm{LST})\cos(\mathrm{LAT}) \qquad (8)$$

The solar zenith angles for any latitude and local solar time consistent with this approximation are shown in Table 4-8. Shown in Tables 4-9, 4-10, 4-11, 4-12 and 4-13 are average conditions for solar zenith angles of 34, 61, 90, 119, and 146° respectively. Conditions appropriate for noon at 16°N (solar zenith angle = 16°) and midnight at 16°N (solar zenith angle = 164°) are given in Tables 4-4 and 4-5 respectively. Thus, by interpolation between these tables, conditions can be rapidly estimated essentially anywhere on the planet.

As may be noted by referring to Tables 4-9 through 4-13, conditions are fairly constant on the dayside, abruptly change near the terminator, and then are fairly constant on the nightside. When estimating conditions at various latitudes, it should be kept in mind that the 150- to 250-km models are based on data obtained principally near 16°N and are consistent with exospheric temperatures and total densities measured by BNMS at 40°S (von Zahn et al., 1980). There is also evidence from measurements at higher and lower altitudes that the atmosphere is strongly controlled by solar zenith angle. For example, Bertaux et al., (1982) report exospheric temperatures

determined on the dayside in the polar regions to be 275 ±25 K at 79°S (Venera 11) and 300 ±25 K at 59°S (Venera 12). These dayside high-latitude temperatures are very close to the dayside low-latitude temperatures determined here from the OAD and ONMS data.

2.5 Standard Deviation From Mean

There are substantial differences between the day- and nightsides in the random variability of the Venus upper atmosphere. Shown in Figure 4-10, for example, is the standard deviation of densities obtained each Earth day from reference densities for each hour of Venus local solar time, based on OAD data. On the Venus dayside, one standard deviation is about ±10% while on the nightside, one standard deviation variations is near ±50%. These variations are in part apparently related to waves propagating upwards from lower in the atmosphere (Keating et al., 1979b). Thermal periodicities of five to six days detected in the atmosphere below 100 km by OIR (Apt and Leung, 1982) were also detected by OAD above 150 km (Keating et al., 1979b). Shown in Table 4-14 is the standard deviation in concentrations obtained each Earth day of individual species on the day- and nightsides derived from ONMS data. The extreme variability on the nightside results in the reference models more accurately representing six-day means than the daily conditions. It should be recalled that the standard error of the mean over nine days is approximately a factor of 3 lower than the daily standard deviation.

2.6 Variations with Solar Activity

The response of the Venus neutral upper atmosphere to solar activity variations has been detected by both OAD measurements (Keating et al., 1981) and ONMS measurements (Hedin et al., 1983). The response is very small compared to the corresponding variations on the Earth. Further evidence of the relative insensitivity of the upper atmosphere to solar activity variations comes from the relatively constant inferred temperatures obtained from day-side Lyman α measurements during low and high solar activity (See Table 4-17). On the other hand, Table 4-17 gives some evidence for a decrease of H concentration with increasing solar activity. Possible short-term systematic variations in the neutral upper atmosphere associated

with fluctuations in the solar wind have also been investigated and are found to be extremely small (Keating et al., 1980) and are neglected here.

The index of solar activity used here is the 10.7-cm flux from the sun in the direction of Venus. Although the 10.7-cm flux is not in the ultraviolet, this wavelength is widely used as a convenient index of variations in solar extreme ultraviolet (EUV) radiation since it can be monitored daily from the Earth's surface. Hedin et al. (1983) have detected variations in composition at 150 km related to solar activity. These variations have been combined with the solar activity variations in temperature indicated in Table 4-2 to give the response of the upper atmosphere to solar activity variations.

A simplified empirical expression for the change in $\log_{10}$ of the species number density n_i, due to solar activity variations is given by the following equation:

$$\Delta \log_{10} n_i \approx A + B + 0.44\, m_i \left(\frac{\Delta T_{\infty,s} + \Delta T_{\infty,\ell}}{T^2} \right) (z - 150) \quad (9)$$

where T = ambient temperature;

A and $\Delta T_{\infty,l}$ are given by Figure 4-11 as functions of $\bar{F}_{10}$;

B and $\Delta T_{\infty,s}$ are given by Figure 4-12 as functions of $F_{10} - \bar{F}_{10}$;

m_i = molecular weight of the i^{th} species;

z = the altitude of measurement above the 6,052-km planetary radius, km;

$\bar{F}_{10}$ = the 81-day mean of 10.7-cm solar flux at 1 astronomical unit divided by 10^{-22} Wm^{-2} Hz^{-1}; and

F_{10} = the daily value of the 10.7-cm solar-activity index at one astronomical unit (determined for the direction of Venus taking into account a 27-day rotation of the Sun) divided by 10^{-22} Wm^{-2} Hz^{-1}.

Figure 4-11 indicates that with an increase in the long-term $\bar{F}_{10}$ from 150 to 200, the exospheric temperature increases 29 K.

On the other hand, Figure 4-12 indicates that a short-term increase in $\bar{F}_{10}$ of 50 units over F_{10} results in only an 18-K increase in exospheric temperature. Thus, as is the case on Earth, the Venus upper atmosphere appears to be more responsive to the longer-term changes in solar activity. It may also be observed that compositional variations are larger for the long-term solar activity variations. However, the user should take into account that a poor sample of long-term variations was obtained over the relatively short interval of observations and that a much better sample of the response to short-term variations was obtained. However, referring to Figure 4-11, the variation in temperature for an increase in $\bar{F}_{10}$ from 70 to 200 units is ~75 K. It is of interest that an update of the Dickinson and Ridley (1977) model incorporating processes providing consistency with Pioneer Venus observations of mean conditions and diurnal variations (Bougher, 1985), but not fit to solar variability predicts a temperature change of $\leq$75 K for this increase in $\bar{F}_{10}$.

3. Models Between 100 km and 150 km

3.1 Measurements

In-situ measurements of composition, temperature, and density below 150 km were obtained down to an altitude of about 130 km at a local time of about 8:30 AM by the BNMS (von Zahn, et al., 1980), and at night by means of the ONMS and OAD experiments down to near 140 km.

In-situ measurements of density and temperature were obtained by SAS3 up to ~130 km, SAS2 up to ~120 km, SAS1 up to ~115 km, and LAS up to ~115 km. Shown in Figure 4-13 are densities obtained on the dayside and the nightside by the BNMS, SAS3, SAS2, OAD, and ONMS. Shown in Figure 4-14 are pressures derived from measurements obtained on the day- and nightsides by the BNMS, SAS3, SAS2, SAS1, LAS, and OAD compared with the model of Dickinson (1972). Shown in Figure 4-15 are temperatures derived from deceleration of the three Pioneer Venus small probes and Veneras 11 and 12. Shown in Figure 4-16 is the Venus morning-side model of von Zahn et al. (1980), based on BNMS data compared with OAD and LAS data. Other relevant measurements between 100 and 150 km are reviewed by Massie et al., (1983). They include ground-based measurements of CO,

ground-based measurements of O_2 ($^1\Delta$) emission at 1.27 μm (Krasnopolsky, 1976; Lawrence et al., 1977), Herzberg II emissions, and NO night-side airglow. The CO measurements, obtained by F. P. Schloerb (see Massie et al., 1983, page 3957) and by Wilson et al. (1981) in the microwave, indicate CO concentrations at 100 km, higher by a factor of 2, on the nightside. The NO airglow in the delta and gamma bands detected by the OUVS (Stewart and Barth, 1979) result from the reaction on the nightside of N and O, which are apparently produced on the dayside and transported to the nightside. The NO airglow occurs near 115 km and is principally between $\pm 30°$ latitude and between midnight and 4 AM.

The eddy-diffusion coefficient on the dayside has been estimated from the BNMS measured vertical distribution of He to be given by the expression $K(z) = An^{-1/2}$ cm^2 s^{-1}, where n is the total number density (cm^{-3}), and $A = 1.4 \times 10^{13}$ (von Zahn et al., 1983). Values of A on the nightside based on NO airglow considerations are estimated to be near 0.8×10^{13} (Gerard et al., 1981). Massie et al., (1983) estimate values of A closer to 1.0×10^{13}. Bougher (1985a) developed a two-dimensional model allowing for both vertical bulk motion and eddy diffusion. Using this approach, much lower eddy coefficients were derived.

In addition, the large-scale dynamic models (Bougher, 1985a) provide a different vertical structure of minor species below 130 km compared to the one-dimensional models. Shown in Figure 4-17(a) are the noon and midnight O and CO concentrations estimated from the two-dimensional model. Transport from the dayside has produced O and CO bulges on the nightside below 125 km.

There are various theoretical estimates of how the photochemistry in the mesosphere will affect concentrations of various species near 100 km. These estimates include the studies of Krasnopolsky and Parshev (1981) and those of Yung and Demore (1982). Shown in Figure 4-17(b) is the estimated composition of the dayside upper atmosphere as modeled by Krasnopolsky and Parshev (1981). Concentrations indicated by dashed lines have been multiplied by a factor of 1,000. The only species in the figure which have been quantitatively detected between 100 and

150 km are CO_2, CO, and O. However, evidence of atomic carbon supports the O_2 concentrations.

3.2 Model Formulation

The problem of the sparsity of measurements on Venus between 100 and 150 km is analogous to the problem on Earth: the altitudes are generally too low for continuous satellite measurements and yet the variations in the region are so complex that many measurements are needed. The potential inaccuracies of extrapolating down from well-measured regions are demonstrated by Massie et al. (1983) in terms of the extreme sensitivity of conditions to the eddy-diffusion coefficient, vertical transport, and chemistry.

The models assume the 150-km mixing ratios given in the 150-to-250-km reference model and make a transition near the homopause (~130 km) to the mixing ratios in the Massie-et-al. (1983) models. The CO_2 profiles are in fair agreement with the OIR temperatures at 100 km (Schofield and Taylor, 1983a), the temperature model of Seiff (1983c) near 115 km, and the temperatures determined from OAD vertical structure and ONMS mixing ratios near 150 km. CO_2 densities are close to the model of Seiff (1983c) from 100 to 115 km and consistent with the 150-250-km reference model at 150 km. The Massie-et-al. (1983) model attempts to take into account chemical production and loss as well as transport processes. Night-side densities and fluxes are consistent with the observed airglow of NO. Since the Massie-et-al. (1983) model did not include mixing ratios of N on the dayside, the mixing ratios near 120 km given by the Hedin- et-al. (1983) model were assumed. These concentrations are higher than those estimated by Krasnopolsky (1985). CO mixing ratios at night were increased by a factor of 2 above those in Massie et al. (1983) at 100 km in order to be in accord with the observed diurnal variation of CO at those altitudes, and to be more in accord with the increased CO concentrations on the nightside given in two-dimensional models (Bougher, 1985a).

3.3 Night-Side and Day-Side Models

Shown in Figures 4-18 and 4-19 are the resulting night-side (7 PM - 5 AM) and day-side (7 AM - 5 PM) reference models re-

spectively for T, ρ, CO_2, O, CO, N_2, He, and N. Shown in Tables 4-15 and 4-16 are the tabulated values for the night-side and day-side reference models, respectively. Included in the tabulation are density (g cm^{-3}), temperature (K), $n(CO_2)$ (cm^{-3}), n(O) (cm^{-3}), n(He) (cm^{-3}), n(N) (cm^{-3}), $n(N_2)$ (cm^{-3}), n(CO)(cm^{-3}), mean molecular weight (moles), total number density (cm^{-3}), pressure (mb), speed of sound (cms^{-1}), mean free path (cm), pressure scale height (km), and density scale height (km). Molecular oxygen concentrations may be estimated assuming O_2/CO_2 ~3 x 10^{-3} (Fox, 1982).

It should be kept in mind that there are substantial latitudinal (Seiff et al., Chapter I of this issue), semidiurnal (F. W. Taylor et al., 1985), and diurnal variations (F. W. Taylor et al., 1985) near 100 km. Thus, although representation of data in terms of day and night is convenient, and justified in light of the lack of data, the actual variations may be somewhat more complex.

3.4 Dynamics

Estimates of the dynamics causing the observed variations in the Venus upper atmosphere have been made using various 1-D, 2-D, and 3-D models. Of particular significance has been the work of Mayr et al. (1980 and 1985), in which transport from the dayside to the nightside, as well as superrotation, has been estimated, and recent work of Dickinson and Bougher (1984), Bougher (1985a), and Dickenson and Bougher (1986), improving the models developed at the National Center for Atmospheric Research in Boulder, Colorado (USA), hereafter called NCAR models.

The NCAR models represent a redevelopment of the computer models described by Dickinson (1972) and Dickinson and Ridley (1977) in light of the recent Pioneer Venus results. In particular, the night-side cryosphere, the low mean global temperature at these altitudes, the lack of an atomic oxygen bulge above 125 km on the nightside, and the magnitude of the night-side helium bulge are taken into consideration in the improved models. General agreement with the observations was achieved with reduced transport across the terminator from the day- to the nightside (see also Mayr et al., 1980 and 1985) by inclusion of a Rayleigh friction term, increased cooling of

the atmosphere through transfer of energy from O impacting on CO_2 with the CO_2 ν_2 = 1 vibrational quanta then escaping to space, and inclusion of vertical eddy diffusion on compositional constituents, especially on the nightside.

The resulting agreement between the 2-D NCAR model (Bougher, 1985) and the 150-km VIRA model on the dayside and nightside is noted in Table 4-3. These entries include 1985 refinements (Bougher, 1985). Shown in Figure 4-20 is the corresponding theoretical total temperature as a function of altitude and solar zenith angle. The temperatures are shown up to the altitude of the exobase. The observed increase of temperatures with altitude on the dayside and the decrease with altitude on the nightside (cryosphere) is clearly reproduced. Shown in Figures 4-21 and 4-22 are the vertical and horizontal velocities respectively as a function of altitude and solar zenith angle. Maximum horizontal velocities near the terminator are calculated to be near 0.2 km/sec as opposed to the much higher velocities in pre-Pioneer Venus calculations.

Three-dimensional models have also been generated recently in order to explain Pioneer Venus results (Mayr et al., 1980 and 1985; Bougher, 1985a). Shown in Figure 4-23 are the NCAR 3-D results at pressure levels (Z) which are related to altitude as indicated in Figure 4-24. The horizontal wind velocities (U) are essentially self-consistent with the values generated in the 2-D model and are essentially symmetrical with respect to the subsolar and antisolar points. When superrotation is taken into account, Mayr et al. (1980, 1985) have shown that the predawn bulges of the lighter species can be explained.

4. Models Between 250 km and 3,500 km

4.1 Measurements

Above 250 km, a number of Lyman α measurements of atomic hydrogen have been obtained from spacecraft since 1967. These include measurements from Venera 4 (Kurt et al., 1968), Mariner 5 (Anderson, 1976), Mariner 10 (Takacs et al., 1980), Venera 9 (Bertaux et al., 1978), Venera 11 and 12 (Bertaux et al., 1982), and Pioneer Venus (Stewart et al., 1979; Paxton et al., 1985). The hydrogen distribution and exospheric temperatures determined from Lyman α data are summarized in Table 4-17

(von Zahn et al., 1983). Note that in addition to the thermal components which have exospheric temperatures consistent with the 150- to 250-km models, nonthermal components with much higher temperatures of ~1000 K have been detected for atomic hydrogen. In-situ measurements of neutral helium concentrations have been obtained up to 650 km (von Zahn et al., 1980). Helium 584-Å measurements have also been obtained (Kumar and Broadfoot, 1975) and (Bertaux et al. 1981 and 1985). Measurements have been obtained from ONMS of composition and OAD of density above 250 km on the dayside.

The nonthermal components of a number of species in addition to H have been detected from OUVS. A nonthermal component for atomic oxygen has been detected on the dayside from 1,304-Å measurements by OUVS (Nagy et al., 1981; Paxton, 1983; Paxton and Stewart, 1984). The OUVS measurement of the 1,657-Å line gives evidence of hot carbon concentrations on the order of 10^3 cm^{-3} at 250 km, with effective non-Maxwellian temperatures of 4,000 K (Paxton, 1983; Nagy et al., 1983). This implies 1% thermal carbon at the exobase consistent with Fox (1982). Measurements of the 1,493-Å line by OUVS gives evidence of hot nitrogen (actually $N(^2D)$) with concentrations of about 10^4 cm^{-3} at 250 km and an effective non-Maxwellian temperature of about 5,500 K (Paxton and Stewart, 1984; Paxton, 1983; Nagy et al., 1983.

Figure 4-25(a) shows the theoretical distribution of nonthermal oxygen atoms in the Venusian exosphere. These atoms are produced near the exobase by the dissociative recombination of O_2^+. The most energetic atoms have initial energies of 3.48 eV and rise to an altitude of 4,300 km. The curve labelled "INITIAL COMPONENT" represents "fresh" atoms that have not undergone collisions; the curve labelled "SPUTTERED COMPONENT" represents those atoms that have been involved in one or more collisions between hot and thermal atoms.

Figure 4-25(b) (Paxton, 1983) compares the predicted limb signal at 1,304 Å with the average of three-orbits'-worth of PV OUVS measurements. The branching ratios of the dissociative recombination process were adjusted to provide good agreement at high altitudes.

Hot carbon atoms are produced by dissociative recombination of CO^+ and as a result of sputtering by hot oxygen atoms. The

sputtering mechanism dominates, as the models in Figure 4-26(a) (Paxton, 1983) show. (In the CO^+ model, the density of CO^+ was calculated using an ion-chemistry model that adequately reproduces the PV OIMS measurements of $CO^+ + N_2^+$).

Figure 4-26(b) (Paxton, 1983) shows the contribution of hot carbon to the PV OUVS limb signal at 1,657 Å. Below 300 km, this signal is composed of the optically thick resonance emission from thermal atomic carbon and a contamination signal from the CO fourth positive system. Above 300 km, the hot carbon component is dominant. The magnitude of the hot carbon signal requires a C:O ratio of about 0.01 at the exobase.

Figure 4-27(a) shows the theoretical distribution of hot N in the Venusian exosphere. The primary source is dissociative recombination of N_2^+, with lesser contributions from sputtering by hot O and from dissociative recombination of NO^+. The model uses ion densities from a theoretical calculation that adequately reproduces the $N_2^+ + CO^+$ density measured by the PV OIMS (Paxton, 1985b).

Hot N atoms in the metastable ^2D state can be observed in resonance scattering at 1,493 Å. Figure 4-27(b) compares the theoretical signal (including contribution from hot $N(^2D)$, thermal $N(^2D)$, and the CO fourth positive system with the PV OUVS limb signal. The hot atom component dominates above 400 km. The excess of measured signal over the model between 200 km and 400 km is due to the effects of multiple scattering which were not included.

4.2 Model Formulation

The philosophy of model formulation was basically to estimate thermal components by extrapolating in-situ measurements and to use airglow measurements to estimate the nonthermal components. Bertaux, et al. (1982) and Paxton et al. (1985) have shown good agreement between their day-side airglow measurements of H and the in-situ measurements of Brinton et al. (1980). The night-side in-situ and airglow measurements of H appear to compare poorly, but the differences may be partially related to variations over the solar cycle (Brinton et al., 1980).

4.3 Day-Side Model (250 to 3,500 km)

Shown in Figure 4-28 is the reference model for the vertical structure above 250 km on the dayside. The thermal O, He, H, and C components are consistent with the exospheric temperatures and upper boundary of the 150- to 250-km noon model. The nonthermal component of H (1,000 K) is consistent with the Venera 11/12 observations (Bertaux et al., 1982). The nonthermal components of O, N, and C are consistent with OUVS observations (Paxton, 1983, 1985a, and 1985b; Paxton and Stewart, 1984; Nagy et al., 1981). As may be observed, the major species changes with increasing altitude from thermal O to thermal He to hot O to hot H. Note that thermal H never appears to predominate. The total density is also shown. If the day-side differences shown in Table 4-17 are related to solar activity, substantial increases in H density may occur near solar minimum.

4.4 Night-Side Model (250 to 3,500 km)

Shown in Figure 4-29 is a model of the vertical structure above 250 km on the nightside. The thermal O, He, and H components are extrapolations from the 150- to 250-km night-side model. The nonthermal component of H (1500 K) (Anderson, 1976) is also shown. Note the theoretical distribution of nonthermal O (hot O) indicated by the dashed line (Nagy et al., 1981). On the nightside, the transition of major components is simply from thermal H to nonthermal H. In the case hot O has concentrations similar to those estimated, it could replace thermal H as the principal species near 2,000 km.

Table 4-1. Spacecraft Measurements of Venus Neutral Upper Atmosphere Above 100 km

Acronym	Experiment	Spacecraft	Measurement
ONMS	Orbiter Neutral Mass Spectrometer	Pioneer Venus Orbiter	CO_2, O, CO, N_2, N, He, T, p, ρ
OAD	Orbiter Atmospheric Drag	Pioneer Venus Orbiter	ρ, H_ρ, T, O, CO_2, p
OUVS	Orbiter Ultraviolet Spectrometer	Pioneer Venus Orbiter	NO, O, (N), He, H, CO, C
OIMS	Orbiter Ion Mass Spectrometer	Pioneer Venus Orbiter	H^+, D^+
OIR	Orbiter Infrared Radiometer	Pioneer Venus Orbiter	T
BNMS	Bus Neutral Mass Spectrometer	Pioneer Venus Bus	He, N_2, CO, CO_2, K_Z, T, p,
SAS3	Accelerometer	Pioneer Venus Night Probe	ρ, T, p
SAS2	Accelerometer	Pioneer Venus Day Probe	ρ, T, p
SAS1	Accelerometer	Pioneer Venus North Probe	ρ, T, p
LAS	Accelerometer	Pioneer Venus Large Probe	ρ, T, p
(V12) EUVS	EUV Spectrometer	Venera 12	H, O, He, O^+, T
(V11) EUVS	EUV Spectrometer	Venera 11	H, O, He, O^+, T
(V9/10) RC	Resonance Cells	Venera 9/10	H, T
(M 10) UVS	Ultraviolet Spectrometer	Mariner 10	H, He, T
(M 5) UVP	Ultraviolet Photometer	Mariner 5	H, O, T
(V 4) UVP	Ultraviolet Photometer	Venera 4	H, O, T
(IUE) UVS	Ultraviolet Spectrometer	International Ultraviolet Explorer	NO, N

Table 4-2. Model Parameters Derived From OAD Drag Data and ONMS 150-km Mixing Ratios

Composition Sensitivity Parameters	
CO_2 multiplier	1.83
O multiplier	1.58
Mean Exospheric Temperature (^oK)	
$\bar{T}_\infty$	229.1
Solar Activity Temperature Parameter ($10^{-22}Wm^{-2}Hz^{-1})^{-1}$	
$\bar{F}_{10}$ parameter	0.137×10^{-2}
F_{10} parameter	0.084×10^{-2}
Diurnal Temperature Parameters	
a_{10}	+0.592
a_{20}	-0.063
a_{30}	-0.234
a_{40}	+0.024
a_{50}	+0.036

Table 4-3. Empirical and Theoretical Calculations of the Concentration of Species Relative to the VIRA Model at 150 km Correcting for Variability

CO_2	O	CO	N_2	N	He	Reference
1.08	1.31	0.87	1.05		1.19	Bougher, 1985 (Dayside)
0.73	1.04	1.12	1.38		0.97	Bougher, 1985 (Nightside)
0.89	1.03	1.03	1.03	1.03	1.03	Hedin, et al., 1983
0.77	1.01	1.52	1.58		1.01	von Zahn et al., 1980
0.98	1.01	1.01	1.52	0.63	0.82	Massie et al., 1983
	1.00					Paxton and Meier, 1985
	0.95					Cravens et al., 1981a
	0.99					Seiff, 1983c
					0.32	Bertaux et al., 1985

Table 4-4. VIRA Model of Composition, Temperature, and Density: 150-250 km, Noon, 16° N ($\bar{F}_{10}$ = 150)

KM.	RHO	T	CO2	O	CO	HE	N	N2	H	MMWT
	g cm^{-3}	K	cm^{-3}	cm^{-3}	cm^{-3}	cm^{-3}	cm^{-3}	cm^{-3}	cm^{-3}	g/mole
150.	.994E-12	246.5	.981E+10	.400E+10	.234E+10	.501E+07	.465E+08	.132E+10	.888E+05	34.2
155.	.450E-12	257.4	.387E+10	.278E+10	.127E+10	.451E+07	.336E+08	.720E+09	.843E+05	31.2
160.	.222E-12	265.0	.160E+10	.198E+10	.718E+09	.410E+07	.249E+08	.406E+09	.809E+05	28.3
165.	.119E-12	270.5	.683E+09	.143E+10	.415E+09	.375E+07	.187E+08	.234E+09	.782E+05	25.6
170.	.677E-13	274.4	.298E+09	.105E+10	.243E+09	.346E+07	.142E+08	.137E+09	.759E+05	23.4
175.	.410E-13	277.1	.132E+09	.776E+09	.144E+09	.319E+07	.109E+08	.815E+08	.740E+05	21.5
180.	.261E-13	279.0	.590E+08	.576E+09	.863E+08	.296E+07	.840E+07	.488E+08	.723E+05	20.1
185.	.173E-13	280.4	.266E+08	.430E+09	.519E+08	.274E+07	.650E+07	.293E+08	.707E+05	19.1
190.	.119E-13	281.4	.121E+08	.322E+09	.314E+08	.255E+07	.504E+07	.177E+08	.693E+05	18.3
195.	.831E-14	282.1	.551E+07	.242E+09	.190E+08	.237E+07	.392E+07	.107E+08	.679E+05	17.7
200.	.594E-14	282.5	.252E+07	.182E+09	.115E+08	.221E+07	.305E+07	.653E+07	.667E+05	17.2
205.	.430E-14	282.9	.116E+07	.137E+09	.703E+07	.205E+07	.238E+07	.397E+07	.654E+05	16.9
210.	.314E-14	283.1	.532E+06	.103E+09	.429E+07	.191E+07	.186E+07	.242E+07	.643E+05	16.6
215.	.232E-14	283.3	.245E+06	.777E+08	.262E+07	.178E+07	.145E+07	.148E+07	.631E+05	16.4
220.	.172E-14	283.4	.113E+06	.587E+08	.160E+07	.166E+07	.113E+07	.905E+06	.620E+05	16.2
225.	.128E-14	283.5	.524E+05	.443E+08	.980E+06	.155E+07	.888E+06	.554E+06	.609E+05	16.0
230.	.961E-15	283.6	.243E+05	.335E+08	.601E+06	.144E+07	.695E+06	.340E+06	.598E+05	15.8
235.	.722E-15	283.6	.113E+05	.253E+08	.368E+06	.135E+07	.544E+06	.208E+06	.588E+05	15.6
240.	.544E-15	283.6	.523E+04	.192E+08	.226E+06	.126E+07	.426E+06	.128E+06	.578E+05	15.4
245.	.411E-15	283.7	.243E+04	.145E+08	.139E+06	.117E+07	.334E+06	.785E+05	.568E+05	15.2
250.	.312E-15	283.7	.113E+04	.110E+08	.855E+05	.109E+07	.262E+06	.483E+05	.558E+05	15.0

Table 4-5. VIRA Model of Composition, Temperature, and Density: 150-250 km, Midnight, 16°N ($\bar{F}_{10}$ = 150)

KM.	RHO	T	CO2	O	CO	HE	N	N2	H	MMWT
	g cm^{-3}	K	cm^{-3}	cm^{-3}	cm^{-3}	cm^{-3}	cm^{-3}	cm^{-3}	cm^{-3}	g/mole
150.	.342E-13	127.4	.710E+08	.851E+09	.724E+08	.189E+08	.580E+07	.591E+08	.164E+08	18.8
155.	.151E-13	127.4	.123E+08	.450E+09	.237E+08	.161E+08	.332E+07	.194E+08	.158E+08	16.8
160.	.729E-14	127.4	.213E+07	.238E+09	.778E+07	.137E+08	.190E+07	.635E+07	.151E+08	15.4
165.	.372E-14	127.4	.371E+06	.126E+09	.256E+07	.117E+08	.109E+07	.209E+07	.145E+08	14.1
170.	.195E-14	127.4	.648E+05	.668E+08	.842E+06	.999E+07	.626E+06	.687E+06	.140E+08	12.7
175.	.105E-14	127.4	.113E+05	.354E+08	.278E+06	.853E+07	.359E+06	.227E+06	.134E+08	10.9
180.	.582E-15	127.4	.199E+04	.188E+08	.918E+05	.728E+07	.207E+06	.749E+05	.129E+08	8.9
185.	.333E-15	127.4	.350E+03	.100E+08	.304E+05	.621E+07	.119E+06	.248E+05	.124E+08	7.0
190.	.199E-15	127.4	.618E+02	.533E+07	.101E+05	.531E+07	.684E+05	.822E+04	.119E+08	5.3
195.	.126E-15	127.4	.109E+02	.284E+07	.335E+04	.453E+07	.394E+05	.273E+04	.115E+08	4.0
200.	.849E-16	127.4	.194E+01	.151E+07	.111E+04	.388E+07	.228E+05	.909E+03	.110E+08	3.1
205.	.614E-16	127.4	.346E+00	.808E+06	.371E+03	.331E+07	.131E+05	.303E+03	.106E+08	2.5
210.	.474E-16	127.4	.617E-01	.432E+06	.124E+03	.283E+07	.759E+04	.101E+03	.102E+08	2.1
215.	.386E-16	127.4	.110E-01	.231E+06	.415E+02	.242E+07	.439E+04	.339E+02	.981E+07	1.9
220.	.328E-16	127.4	.198E-02	.124E+06	.139E+02	.207E+07	.254E+04	.113E+02	.943E+07	1.7
225.	.286E-16	127.4	.356E-03	.662E+05	.467E+01	.177E+07	.147E+04	.381E+01	.907E+07	1.6
230.	.255E-16	127.4	.643E-04	.355E+05	.157E+01	.152E+07	.854E+03	.128E+01	.873E+07	1.5
235.	.231E-16	127.4	.116E-04	.191E+05	.529E+00	.130E+07	.496E+03	.432E+00	.840E+07	1.4
240.	.211E-16	127.4	.211E-05	.103E+05	.179E+00	.111E+07	.288E+03	.146E+00	.808E+07	1.4
245.	.194E-16	127.4	.384E-06	.552E+04	.604E-01	.952E+06	.167E+03	.492E-01	.777E+07	1.3
250.	.179E-16	127.4	.700E-07	.297E+04	.204E-01	.816E+06	.975E+02	.167E-01	.747E+07	1.3

Table 4-6. VIRA Model of Other Parameters: 150-250 km, Noon, 16°N ($\bar{F}_{10}$ = 150)

KM.	NTOT	P(MB)	SS	MFP	HP	HRHO
	cm^{-3}	mb	$cm\ sec^{-1}$	cm	km	km
150.	.175E+11	.596E-06	.290E+05	.141E+05	7.1	6.0
155.	.868E+10	.308E-06	.310E+05	.309E+05	8.1	6.7
160.	.473E+10	.173E-06	.330E+05	.622E+05	9.2	7.5
165.	.279E+10	.104E-06	.351E+05	.116E+06	10.4	8.4
170.	.175E+10	.661E-07	.370E+05	.203E+06	11.6	9.5
175.	.115E+10	.439E-07	.387E+05	.335E+06	12.8	10.6
180.	.782E+09	.301E-07	.402E+05	.528E+06	13.8	11.7
185.	.547E+09	.212E-07	.414E+05	.800E+06	14.6	12.7
190.	.391E+09	.152E-07	.423E+05	.118E+07	15.4	13.7
195.	.283E+09	.110E-07	.431E+05	.169E+07	15.9	14.5
200.	.208E+09	.809E-08	.437E+05	.237E+07	16.4	15.2
205.	.153E+09	.599E-08	.442E+05	.329E+07	16.8	15.8
210.	.114E+09	.446E-08	.446E+05	.452E+07	17.1	16.2
215.	.854E+08	.334E-08	.449E+05	.613E+07	17.4	16.6
220.	.642E+08	.251E-08	.452E+05	.827E+07	17.7	16.9
225.	.484E+08	.189E-08	.455E+05	.111E+08	17.9	17.2
230.	.367E+08	.143E-08	.457E+05	.147E+08	18.1	17.4
235.	.279E+08	.109E-08	.460E+05	.195E+08	18.4	17.6
240.	.213E+08	.832E-09	.463E+05	.256E+08	18.6	17.8
245.	.163E+08	.638E-09	.466E+05	.335E+08	18.9	17.9
250.	.125E+08	.491E-09	.470E+05	.436E+08	19.2	18.1

Table 4-7. VIRA Model of Other Parameters: 150-250 km, Midnight, 16°N ($\bar{F}_{10}$ = 150)

KM.	NTOT	P(MB)	SS	MFP	HP	HRHO
	cm^{-3}	mb	$cm\ sec^{-1}$	cm	km	km
150.	.109E+10	.192E-07	.281E+05	.407E+06	6.7	5.6
155.	.540E+09	.950E-08	.297E+05	.922E+06	7.5	6.6
160.	.285E+09	.501E-08	.310E+05	.188E+07	8.2	7.2
165.	.158E+09	.278E-08	.324E+05	.360E+07	8.9	7.6
170.	.930E+08	.163E-08	.342E+05	.653E+07	10.0	7.9
175.	.583E+08	.102E-08	.369E+05	.112E+08	11.6	8.3
180.	.394E+08	.692E-09	.408E+05	.180E+08	14.2	8.7
185.	.288E+08	.506E-09	.461E+05	.270E+08	18.2	9.3
190.	.227E+08	.398E-09	.529E+05	.375E+08	24.0	10.2
195.	.189E+08	.332E-09	.608E+05	.488E+08	31.7	11.7
200.	.164E+08	.289E-09	.691E+05	.600E+08	41.0	14.0
205.	.147E+08	.259E-09	.769E+05	.707E+08	50.8	17.3
210.	.135E+08	.237E-09	.836E+05	.810E+08	60.3	21.9
215.	.125E+08	.219E-09	.892E+05	.909E+08	68.6	27.5
220.	.116E+08	.204E-09	.935E+05	.101E+09	75.5	34.0
225.	.109E+08	.192E-09	.969E+05	.110E+09	81.2	40.6
230.	.103E+08	.181E-09	.996E+05	.120E+09	86.0	46.9
235.	.971E+07	.171E-09	.102E+06	.130E+09	90.0	52.5
240.	.920E+07	.162E-09	.104E+06	.140E+09	93.5	57.4
245.	.873E+07	.153E-09	.105E+06	.150E+09	96.6	61.7
250.	.829E+07	.146E-09	.107E+06	.161E+09	99.5	65.6

Table 4-8. Approximate Solar Zenith Angle for Local Solar Time and Latitude

	Local Solar Time											
Lat.	12	14	16	18	20	22	0	2	4	6	8	10
0	0	30	60	90	120	150	180	150	120	90	60	30
15	15	33	61	90	119	147	165	147	119	90	61	33
30	30	41	65	90	116	139	150	139	116	90	65	41
45	45	52	69	90	111	128	135	128	111	90	69	52
60	60	64	76	90	104	116	120	116	104	90	76	64
75	75	77	83	90	97	103	105	103	97	90	83	77
90	90	90	90	90	90	90	90	90	90	90	90	90

Table 4-9. VIRA Model 150-250 km, SZA = 34° (2 PM and 10 AM at 16°N)

KM.	RHO	T	CO2	O	CO	HE	N	N2	H	MMWT
	g cm^{-3}	K	cm^{-3}	cm^{-3}	cm^{-3}	cm^{-3}	cm^{-3}	cm^{-3}	cm^{-3}	g/mole
150.	.680E-12	250.4	.628E+10	.349E+10	.174E+10	.464E+07	.377E+08	.100E+10	.112E+06	32.6
155.	.319E-12	261.8	.251E+10	.243E+10	.957E+09	.417E+07	.274E+08	.552E+09	.106E+06	29.6
160.	.164E-12	269.8	.105E+10	.174E+10	.545E+09	.380E+07	.203E+08	.314E+09	.101E+06	26.8
165.	.905E-13	275.5	.456E+09	.126E+10	.317E+09	.348E+07	.154E+08	.183E+09	.980E+05	24.3
170.	.535E-13	279.5	.202E+09	.931E+09	.188E+09	.321E+07	.117E+08	.108E+09	.952E+05	22.3
175.	.335E-13	282.4	.906E+08	.692E+09	.112E+09	.297E+07	.903E+07	.648E+08	.928E+05	20.7
180.	.219E-13	284.4	.411E+08	.517E+09	.679E+08	.275E+07	.699E+07	.391E+08	.907E+05	19.5
185.	.148E-13	285.9	.188E+08	.388E+09	.412E+08	.256E+07	.543E+07	.238E+08	.888E+05	18.6
190.	.103E-13	286.9	.868E+07	.292E+09	.251E+08	.238E+07	.423E+07	.145E+08	.870E+05	18.0
195.	.736E-14	287.6	.402E+07	.220E+09	.154E+08	.222E+07	.331E+07	.886E+07	.853E+05	17.5
200.	.532E-14	288.1	.187E+07	.166E+09	.943E+07	.206E+07	.259E+07	.544E+07	.837E+05	17.1
205.	.389E-14	288.5	.869E+06	.126E+09	.580E+07	.192E+07	.203E+07	.334E+07	.822E+05	16.8
210.	.288E-14	288.7	.406E+06	.954E+08	.357E+07	.180E+07	.159E+07	.206E+07	.808E+05	16.5
215.	.214E-14	288.9	.190E+06	.724E+08	.220E+07	.167E+07	.125E+07	.127E+07	.793E+05	16.3
220.	.160E-14	289.0	.890E+05	.549E+08	.136E+07	.156E+07	.981E+06	.783E+06	.780E+05	16.1
225.	.120E-14	289.1	.418E+05	.417E+08	.840E+06	.146E+07	.771E+06	.484E+06	.766E+05	15.9
230.	.905E-15	289.2	.197E+05	.317E+08	.520E+06	.136E+07	.606E+06	.300E+06	.753E+05	15.8
235.	.684E-15	289.2	.925E+04	.241E+08	.322E+06	.127E+07	.477E+06	.185E+06	.740E+05	15.6
240.	.519E-15	289.3	.436E+04	.183E+08	.199E+06	.119E+07	.376E+06	.115E+06	.728E+05	15.4
245.	.394E-15	289.3	.206E+04	.140E+08	.124E+06	.111E+07	.296E+06	.713E+05	.715E+05	15.2
250.	.300E-15	289.3	.974E+03	.106E+08	.768E+05	.104E+07	.233E+06	.443E+05	.703E+05	15.0

Table 4-10. VIRA Model 150-250 km, SZA = 61° (4 PM and 8 AM at 16°N)

KM.	RHO	T	CO2	O	CO	HE	N	N2	H	MMWT
	g cm^{-3}	K	cm^{-3}	cm^{-3}	cm^{-3}	cm^{-3}	cm^{-3}	cm^{-3}	cm^{-3}	g/mole
150.	.548E-12	250.7	.523E+10	.278E+10	.115E+10	.399E+07	.303E+08	.834E+09	.317E+06	33.0
155.	.255E-12	262.8	.209E+10	.193E+10	.630E+09	.358E+07	.219E+08	.457E+09	.300E+06	29.9
160.	.130E-12	271.3	.879E+09	.138E+10	.359E+09	.326E+07	.163E+08	.260E+09	.288E+06	27.0
165.	.717E-13	277.4	.382E+09	.101E+10	.209E+09	.298E+07	.123E+08	.152E+09	.278E+06	24.5
170.	.423E-13	281.7	.170E+09	.741E+09	.124E+09	.275E+07	.941E+07	.902E+08	.270E+06	22.4
175.	.264E-13	284.7	.767E+08	.552E+09	.747E+08	.255E+07	.726E+07	.542E+08	.263E+06	20.7
180.	.173E-13	286.8	.350E+08	.413E+09	.452E+08	.236E+07	.563E+07	.328E+08	.257E+06	19.5
185.	.118E-13	288.4	.161E+08	.311E+09	.276E+08	.220E+07	.438E+07	.200E+08	.251E+06	18.6
190.	.822E-14	289.4	.749E+07	.234E+09	.169E+08	.204E+07	.342E+07	.123E+08	.246E+06	17.9
195.	.587E-14	290.2	.349E+07	.177E+09	.104E+08	.190E+07	.268E+07	.753E+07	.242E+06	17.4
200.	.426E-14	290.7	.163E+07	.134E+09	.639E+07	.177E+07	.210E+07	.464E+07	.237E+06	17.0
205.	.313E-14	291.1	.765E+06	.102E+09	.395E+07	.166E+07	.165E+07	.287E+07	.233E+06	16.7
210.	.232E-14	291.4	.360E+06	.773E+08	.244E+07	.155E+07	.130E+07	.177E+07	.229E+06	16.4
215.	.173E-14	291.6	.169E+06	.588E+08	.151E+07	.144E+07	.102E+07	.110E+07	.225E+06	16.2
220.	.130E-14	291.7	.800E+05	.447E+08	.938E+06	.135E+07	.803E+06	.681E+06	.221E+06	16.0
225.	.978E-15	291.8	.378E+05	.341E+08	.582E+06	.126E+07	.633E+06	.423E+06	.217E+06	15.8
230.	.740E-15	291.9	.179E+05	.260E+08	.362E+06	.118E+07	.499E+06	.263E+06	.213E+06	15.6
235.	.561E-15	291.9	.849E+04	.198E+08	.225E+06	.110E+07	.393E+06	.163E+06	.210E+06	15.4
240.	.427E-15	292.0	.403E+04	.151E+08	.140E+06	.103E+07	.310E+06	.102E+06	.206E+06	15.2
245.	.325E-15	292.0	.192E+04	.115E+08	.872E+05	.959E+06	.245E+06	.633E+05	.203E+06	15.0
250.	.249E-15	292.0	.912E+03	.879E+07	.544E+05	.896E+06	.193E+06	.395E+05	.199E+06	14.7

Table 4-11. VIRA Model 150-250 km, SZA = 90° (6 AM and 6 PM)

KM.	RHO	T	CO2	O	CO	HE	N	N2	H	MMWT
	g cm^{-3}	K	cm^{-3}	cm^{-3}	cm^{-3}	cm^{-3}	cm^{-3}	cm^{-3}	cm^{-3}	g/mole
150.	.141E-12	201.5	.104E+10	.144E+10	.319E+09	.196E+08	.123E+08	.242E+09	.181E+07	27.6
155.	.622E-13	209.8	.337E+09	.932E+09	.153E+09	.173E+08	.839E+07	.116E+09	.172E+07	23.9
160.	.314E-13	215.7	.115E+09	.619E+09	.765E+08	.155E+08	.585E+07	.581E+08	.164E+07	21.2
165.	.175E-13	219.9	.406E+08	.419E+09	.392E+08	.140E+08	.414E+07	.297E+08	.158E+07	19.2
170.	.105E-13	222.8	.147E+08	.287E+09	.204E+08	.126E+08	.297E+07	.155E+08	.153E+07	17.9
175.	.667E-14	224.9	.539E+07	.198E+09	.108E+08	.115E+08	.215E+07	.817E+07	.149E+07	16.9
180.	.438E-14	226.4	.201E+07	.138E+09	.572E+07	.105E+08	.156E+07	.434E+07	.145E+07	16.2
185.	.295E-14	227.5	.753E+06	.962E+08	.306E+07	.955E+07	.114E+07	.232E+07	.141E+07	15.5
190.	.202E-14	228.2	.285E+06	.674E+08	.165E+07	.872E+07	.834E+06	.125E+07	.137E+07	15.0
195.	.141E-14	228.7	.108E+06	.473E+08	.888E+06	.798E+07	.612E+06	.675E+06	.134E+07	14.4
200.	.988E-15	229.1	.413E+05	.333E+08	.481E+06	.730E+07	.450E+06	.365E+06	.131E+07	13.8
205.	.700E-15	229.4	.158E+05	.235E+08	.261E+06	.669E+07	.331E+06	.198E+06	.128E+07	13.1
210.	.500E-15	229.6	.606E+04	.166E+08	.142E+06	.613E+07	.244E+06	.108E+06	.125E+07	12.3
215.	.361E-15	229.7	.233E+04	.117E+08	.772E+05	.562E+07	.180E+06	.586E+05	.123E+07	11.5
220.	.262E-15	229.8	.900E+03	.827E+07	.421E+05	.515E+07	.133E+06	.320E+05	.120E+07	10.7
225.	.193E-15	229.9	.348E+03	.585E+07	.230E+05	.472E+07	.982E+05	.175E+05	.117E+07	9.8
230.	.143E-15	229.9	.135E+03	.414E+07	.126E+05	.433E+07	.726E+05	.954E+04	.115E+07	8.9
235.	.108E-15	229.9	.522E+02	.294E+07	.688E+04	.397E+07	.537E+05	.522E+04	.112E+07	8.0
240.	.826E-16	230.0	.203E+02	.208E+07	.377E+04	.365E+07	.397E+05	.286E+04	.110E+07	7.2
245.	.641E-16	230.0	.789E+01	.148E+07	.207E+04	.335E+07	.294E+05	.157E+04	.108E+07	6.5
250.	.506E-16	230.0	.307E+01	.105E+07	.113E+04	.307E+07	.218E+05	.861E+03	.105E+07	5.9

Table 4-12. VIRA Model 150-250 km, SZA = 119° (8 PM and 4 AM at 16°N)

KM.	RHO	T	CO2	O	CO	HE	N	N2	H	MMWT
	g cm^{-3}	K	cm^{-3}	cm^{-3}	cm^{-3}	cm^{-3}	cm^{-3}	cm^{-3}	cm^{-3}	g/mole
150.	.473E-13	138.5	.721E+08	.107E+10	.131E+09	.118E+09	.697E+07	.137E+09	.593E+08	17.8
155.	.222E-13	139.2	.144E+08	.595E+09	.469E+08	.102E+09	.416E+07	.489E+08	.569E+08	15.4
160.	.113E-13	139.8	.289E+07	.331E+09	.169E+08	.880E+08	.249E+07	.176E+08	.547E+08	13.3
165.	.617E-14	140.1	.587E+06	.185E+09	.613E+07	.760E+08	.150E+07	.638E+07	.527E+08	11.3
170.	.352E-14	140.4	.120E+06	.104E+09	.223E+07	.658E+08	.903E+06	.232E+07	.507E+08	9.4
175.	.210E-14	140.6	.247E+05	.584E+08	.815E+06	.569E+08	.545E+06	.849E+06	.489E+08	7.6
180.	.132E-14	140.7	.510E+04	.329E+08	.298E+06	.493E+08	.330E+06	.311E+06	.472E+08	6.1
185.	.867E-15	140.8	.106E+04	.186E+08	.110E+06	.427E+08	.200E+06	.114E+06	.455E+08	4.9
190.	.604E-15	140.8	.220E+03	.105E+08	.404E+05	.370E+08	.121E+06	.421E+05	.439E+08	4.0
195.	.444E-15	140.9	.460E+02	.593E+07	.149E+05	.321E+08	.737E+05	.155E+05	.423E+08	3.3
200.	.344E-15	140.9	.964E+01	.336E+07	.551E+04	.278E+08	.448E+05	.574E+04	.408E+08	2.9
205.	.277E-15	140.9	.202E+01	.190E+07	.204E+04	.242E+08	.273E+05	.213E+04	.394E+08	2.5
210.	.232E-15	141.0	.427E+00	.108E+07	.758E+03	.210E+08	.166E+05	.790E+03	.380E+08	2.3
215.	.198E-15	141.0	.901E-01	.614E+06	.282E+03	.182E+08	.101E+05	.294E+03	.367E+08	2.2
220.	.173E-15	141.0	.191E-01	.349E+06	.105E+03	.158E+08	.618E+04	.109E+03	.354E+08	2.0
225.	.153E-15	141.0	.405E-02	.199E+06	.391E+02	.137E+08	.377E+04	.408E+02	.342E+08	1.9
230.	.137E-15	141.0	.862E-03	.113E+06	.146E+02	.119E+08	.231E+04	.152E+02	.330E+08	1.8
235.	.124E-15	141.0	.184E-03	.646E+05	.547E+01	.104E+08	.141E+04	.570E+01	.319E+08	1.8
240.	.112E-15	141.0	.394E-04	.368E+05	.205E+01	.901E+07	.864E+03	.214E+01	.308E+08	1.7
245.	.102E-15	141.0	.844E-05	.210E+05	.770E+00	.783E+07	.529E+03	.802E+00	.297E+08	1.6
250.	.932E-16	141.0	.181E-05	.120E+05	.289E+00	.681E+07	.324E+03	.302E+00	.287E+08	1.6

Table 4-13. VIRA Model 150-250 km, SZA = 146° (10 PM and 2 AM at 16°N)

KM.	RHO	T	CO2	O	CO	HE	N	N2	H	MMWT
	g cm^{-3}	K	cm^{-3}	cm^{-3}	cm^{-3}	cm^{-3}	cm^{-3}	cm^{-3}	cm^{-3}	g/mole
150.	.465E-13	123.5	.528E+08	.114E+10	.997E+08	.699E+08	.705E+07	.153E+09	.376E+08	18.0
155.	.206E-13	123.5	.865E+07	.590E+09	.315E+08	.593E+08	.396E+07	.483E+08	.361E+08	15.9
160.	.984E-14	123.5	.142E+07	.306E+09	.998E+07	.504E+08	.223E+07	.153E+08	.347E+08	14.1
165.	.497E-14	123.5	.234E+06	.159E+09	.317E+07	.427E+08	.126E+07	.485E+07	.333E+08	12.3
170.	.262E-14	123.5	.386E+05	.824E+08	.101E+07	.363E+08	.708E+06	.154E+07	.319E+08	10.3
175.	.144E-14	123.5	.639E+04	.429E+08	.321E+06	.308E+08	.400E+06	.491E+06	.307E+08	8.2
180.	.833E-15	123.5	.106E+04	.223E+08	.102E+06	.262E+08	.226E+06	.157E+06	.294E+08	6.4
185.	.510E-15	123.5	.177E+03	.116E+08	.327E+05	.222E+08	.128E+06	.501E+05	.283E+08	4.9
190.	.335E-15	123.5	.296E+02	.607E+07	.105E+05	.189E+08	.722E+05	.160E+05	.271E+08	3.9
195.	.235E-15	123.5	.495E+01	.317E+07	.336E+04	.161E+08	.409E+05	.514E+04	.261E+08	3.1
200.	.177E-15	123.5	.832E+00	.166E+07	.108E+04	.137E+08	.232E+05	.165E+04	.250E+08	2.6
205.	.140E-15	123.5	.140E+00	.867E+06	.348E+03	.116E+08	.132E+05	.532E+03	.240E+08	2.3
210.	.116E-15	123.5	.237E-01	.454E+06	.112E+03	.988E+07	.747E+04	.172E+03	.231E+08	2.1
215.	.991E-16	123.5	.401E-02	.238E+06	.362E+02	.841E+07	.425E+04	.555E+02	.222E+08	1.9
220.	.863E-16	123.5	.682E-03	.125E+06	.117E+02	.716E+07	.242E+04	.180E+02	.213E+08	1.8
225.	.762E-16	123.5	.116E-03	.657E+05	.380E+01	.610E+07	.138E+04	.583E+01	.204E+08	1.7
230.	.680E-16	123.5	.199E-04	.345E+05	.124E+01	.519E+07	.785E+03	.189E+01	.196E+08	1.6
235.	.612E-16	123.5	.340E-05	.182E+05	.402E+00	.442E+07	.448E+03	.616E+00	.189E+08	1.6
240.	.554E-16	123.5	.585E-06	.959E+04	.131E+00	.377E+07	.256E+03	.201E+00	.181E+08	1.5
245.	.504E-16	123.5	.101E-06	.506E+04	.428E-01	.321E+07	.146E+03	.656E-01	.174E+08	1.5
250.	.460E-16	123.5	.174E-07	.267E+04	.140E-01	.274E+07	.836E+02	.215E-01	.167E+08	1.4

Table 4-14. Standard Deviation (%) of Species on the Dayside and the Nightside

Species	Day	Night
O	15	61
N	17	55
N_2	15	51
CO	16	62
CO_2	19	63
He	23	56

Table 4-15. VIRA Night-Side Reference Model 100-150 km

ALT	RHO	T	CO2	O	CO	HE	N	N2	M	NTOT	P	SS	MFP	HP	HRHO
150.	.342E-13	127.4	.710E+08	.851E+09	.724E+08	.189E+08	.580E+07	.591E+08	19.1	.108E+10	.190E-07	.279E+05	.408E+06	6.6	5.5
145.	.919E-13	127.4	.411E+09	.161E+10	.221E+09	.221E+08	.101E+08	.180E+09	22.5	.246E+10	.432E-07	.257E+05	.152E+06	5.6	4.5
140.	.313E-12	127.4	.238E+10	.304E+10	.676E+09	.223E+08	.177E+08	.564E+09	28.1	.670E+10	.118E-06	.230E+05	.452E+05	4.4	3.7
135.	.136E-11	127.5	.137E+11	.630E+10	.206E+10	.250E+08	.318E+08	.196E+10	33.9	.241E+11	.424E-06	.209E+05	.105E+05	3.7	3.2
130.	.685E-11	127.6	.794E+11	.155E+11	.625E+10	.377E+08	.861E+08	.734E+10	38.0	.109E+12	.191E-05	.198E+05	.211E+04	3.3	3.0
125.	.369E-10	128.0	.457E+12	.467E+11	.190E+11	.761E+08	.253E+09	.298E+11	40.2	.553E+12	.976E-05	.193E+05	.396E+03	3.1	3.0
120.	.202E-09	129.0	.260E+13	.133E+12	.569E+11	.187E+09	.665E+09	.135E+12	41.7	.292E+13	.521E-04	.190E+05	.725E+02	3.0	3.0
115.	.109E-08	131.0	.144E+14	.256E+12	.167E+12	.555E+09	.699E+09	.640E+12	42.7	.154E+14	.279E-03	.189E+05	.134E+02	3.0	3.0
110.	.544E-08	138.0	.722E+14	.279E+12	.427E+12	.164E+10	.127E+09	.304E+13	43.2	.760E+14	.145E-02	.193E+05	.270E+01	3.1	3.3
105.	.221E-07	156.0	.294E+15	.255E+12	.806E+12	.423E+10	.156E+08	.114E+14	43.3	.307E+15	.661E-02	.205E+05	.668E+00	3.5	3.7
100.	.803E-07	170.0	.107E+16	.218E+12	.108E+13	.100E+11	.172E+07	.396E+14	43.4	.111E+16	.261E-01	.214E+05	.184E+00	3.8	3.9

Table 4-16. VIRA Day-Side Reference Model 100-150 km

ALT	RHO	T	CO2	O	CO	HE	N	N2	M	NTOT	P	SS	MFP	HP	HRHO
150.	.994E-12	246.5	.981E+10	.401E+10	.234E+10	.502E+07	.465E+08	.132E+10	34.2	.175E+11	.596E-06	.290E+05	.141E+05	7.1	6.0
145.	.237E-11	236.0	.259E+11	.583E+10	.439E+10	.565E+07	.649E+08	.248E+10	36.9	.387E+11	.126E-05	.273E+05	.600E+04	6.3	5.5
140.	.613E-11	225.0	.717E+11	.913E+10	.842E+10	.703E+07	.902E+08	.554E+10	38.9	.949E+11	.295E-05	.259E+05	.234E+04	5.7	5.1
135.	.169E-10	215.0	.207E+12	.154E+11	.164E+11	.106E+08	.124E+09	.134E+11	40.4	.253E+12	.750E-05	.249E+05	.852E+03	5.2	4.8
130.	.497E-10	206.0	.626E+12	.276E+11	.326E+11	.185E+08	.172E+09	.355E+11	41.4	.722E+12	.205E-04	.241E+05	.292E+03	4.9	4.5
125.	.154E-09	198.0	.198E+13	.442E+11	.668E+11	.365E+08	.200E+09	.104E+12	42.2	.219E+13	.599E-04	.234E+05	.948E+02	4.6	4.3
120.	.508E-09	189.0	.662E+13	.120E+12	.143E+12	.819E+08	.130E+09	.323E+12	42.5	.720E+13	.188E-03	.228E+05	.288E+02	4.3	4.1
115.	.176E-08	182.0	.231E+14	.232E+12	.329E+12	.220E+09	.449E+08	.106E+13	42.8	.247E+14	.620E-03	.222E+05	.835E+01	4.1	4.0
110.	.621E-08	178.0	.821E+14	.345E+12	.667E+12	.681E+09	.686E+06	.357E+13	43.1	.867E+14	.213E-02	.219E+05	.237E+01	4.0	3.9
105.	.225E-07	175.0	.299E+15	.317E+12	.698E+12	.229E+10	.251E+06	.129E+14	43.3	.313E+15	.756E-02	.217E+05	.654E+00	3.9	3.9
100.	.814E-07	175.0	.108E+16	.127E+12	.542E+12	.781E+10	.458E+04	.461E+14	43.3	.113E+16	.273E-01	.217E+05	.181E+00	3.9	3.9

Table 4-17. Hydrogen Distribution in Venus Exosphere from Lyman α Data (Bertaux et al., 1981)

	Mariner 5[b]	Mariner 10[c]	Venera 11, 12[d]
Thermal Component			
Dayside temperature (K)	275 ± 50	275 ± 50	300
Dayside density[a] (cm^{-3})	$(2 \pm 1) \times 10^5$	1.5×10^5	$4^{+3}_{-2} \times 10^4$
Nightside temperature (K)	150 ± 50	150 ± 25	—
Nightside density[a] (cm^{-3})	$(2 \pm 1) \times 10^5$	$(1.0 \pm 0.5) \times 10^5$	—
Nonthermal Component			
Dayside temperature (K)	1020 ± 100	1250 ± 100	1000
Dayside density[a] (cm^{-3})	1.3×10^3	$(5 \pm 1) \times 10^2$	1×10^3
Nightside temperature (K)	1500 ± 200	—	
Nightside density[a] (cm^{-3})	1.0×10^3	—	
Solar 10.7 cm flux	120	73	
Solar zenith angle	0°	60°	80°

[a]All densities are referred to the critical level assumed at 255 km altitude.
[b]See Anderson 1976.
[c]See Takacs et al. 1980.
[d]See Bertaux et al. 1982.

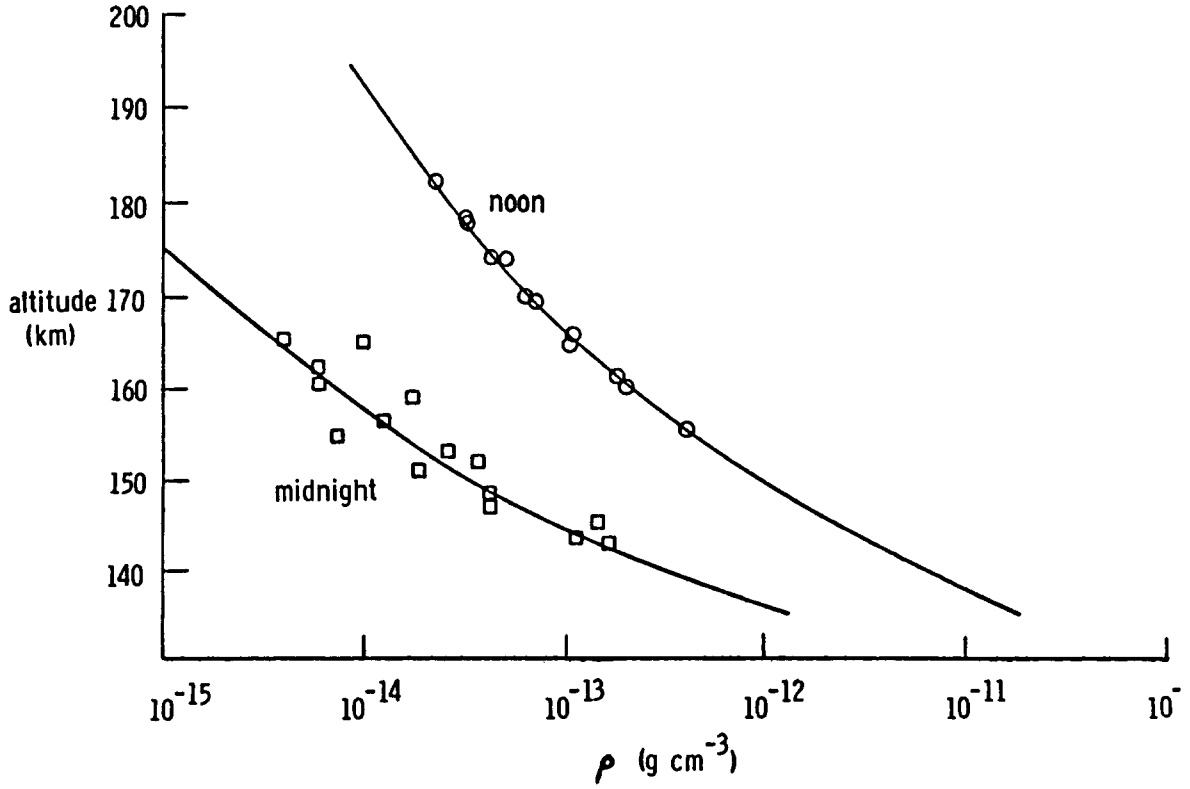

Figure 4-1. Comparison of VIRA Model with OAD-Determined Atmospheric Densities

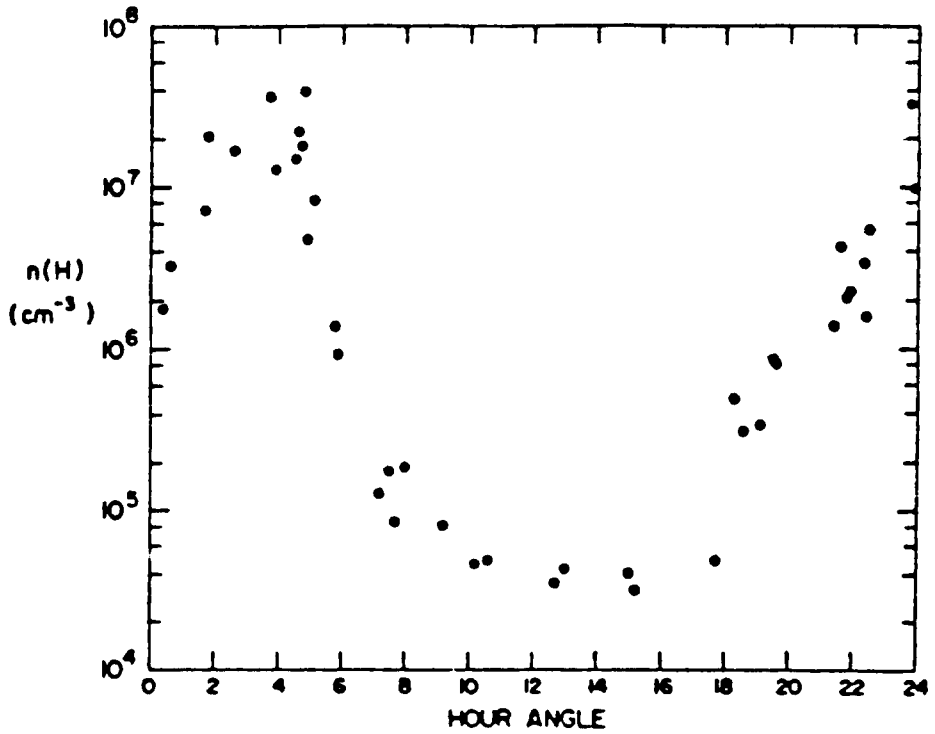

Figure 4-2. Diurnal Variation of n(H) Near 165 km from In-Situ Measurements of $n(H^+)$, $n(O^+)$, h(O) and the Neutral Gas and Ion Temperatures (Brinton et al., 1980)

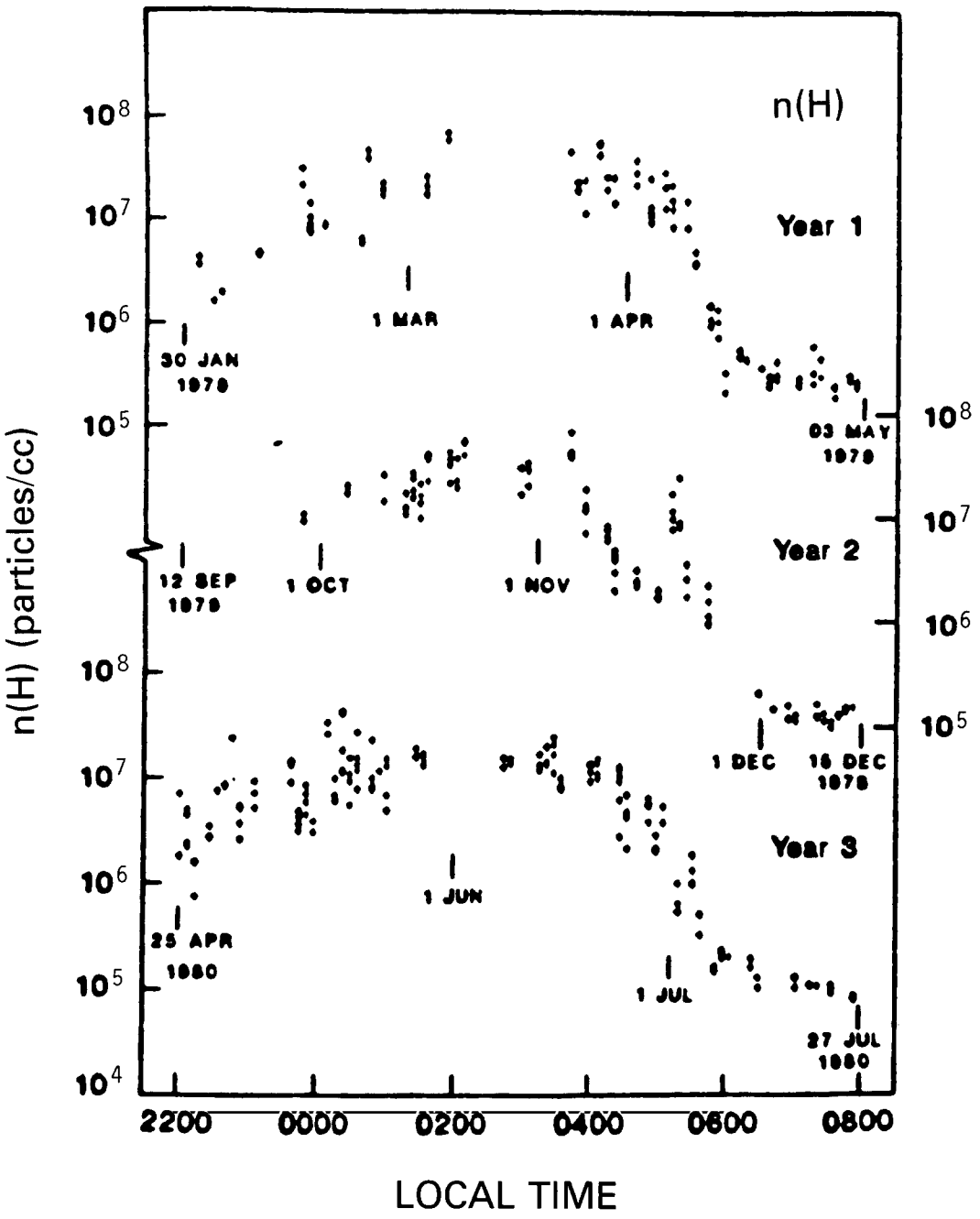

Figure 4-3. Diurnal Variation of n(H) Normalized to 165 km from In-Situ Measurements for Three Diurnal Cycles Observed between 1979 and 1980 (H. A. Taylor, Jr. et al., 1985)

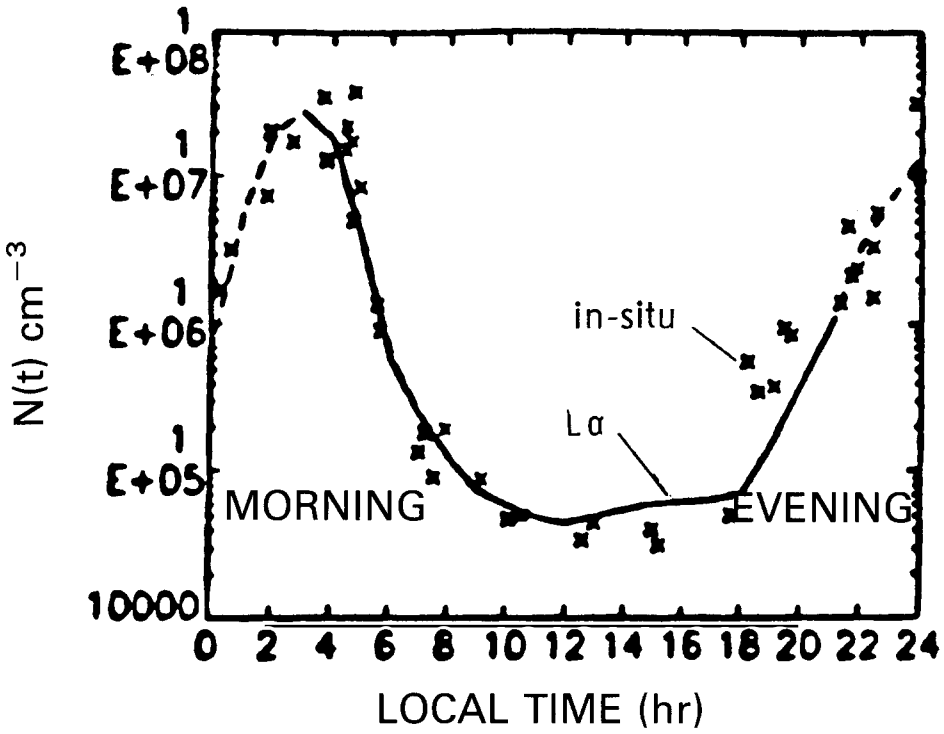

Figure 4-4. Diurnal Distribution of n(H) at 165 km Derived from OUVS Lyman α Measurements (solid line) Compared to In-Situ Measurements (X). The dashed curve represents the projected variation, which is at this point largely speculative (Paxton et al., 1985).

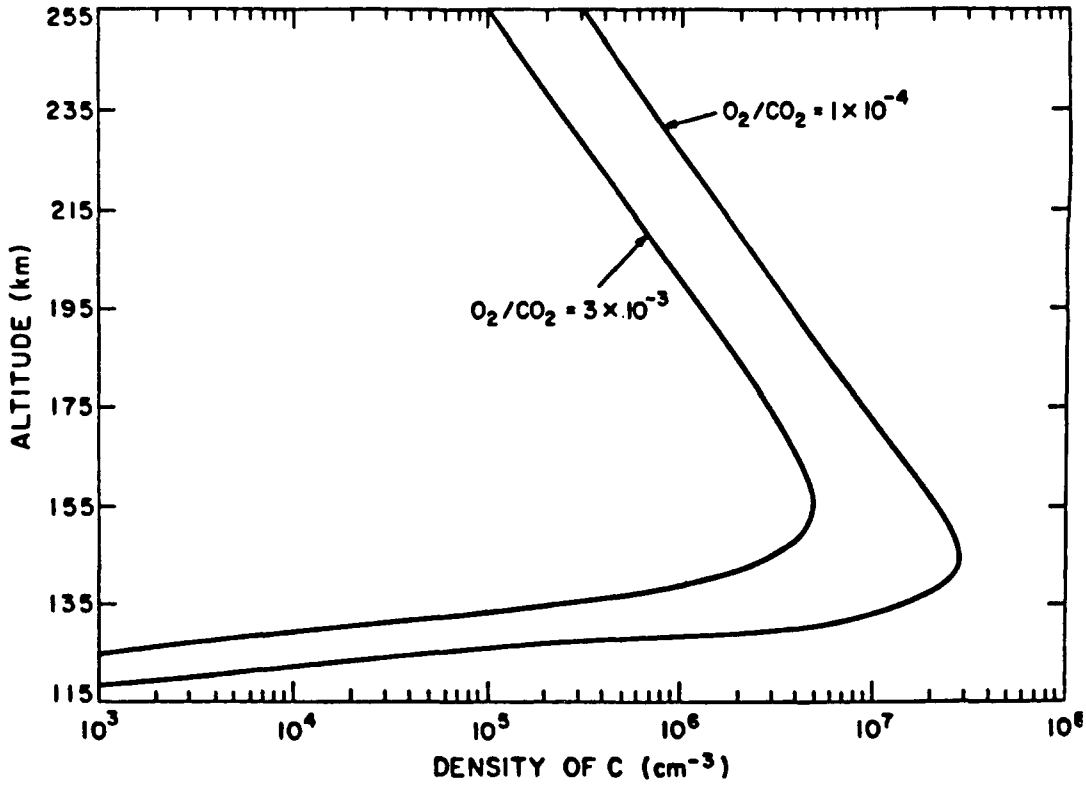

Figure 4-5. Vertical Distribution of n(C) for Two O_2 to CO_2 Ratios (Fox, 1982). The chosen O_2 to CO_2 ratio is 3 x 10^{-3}.

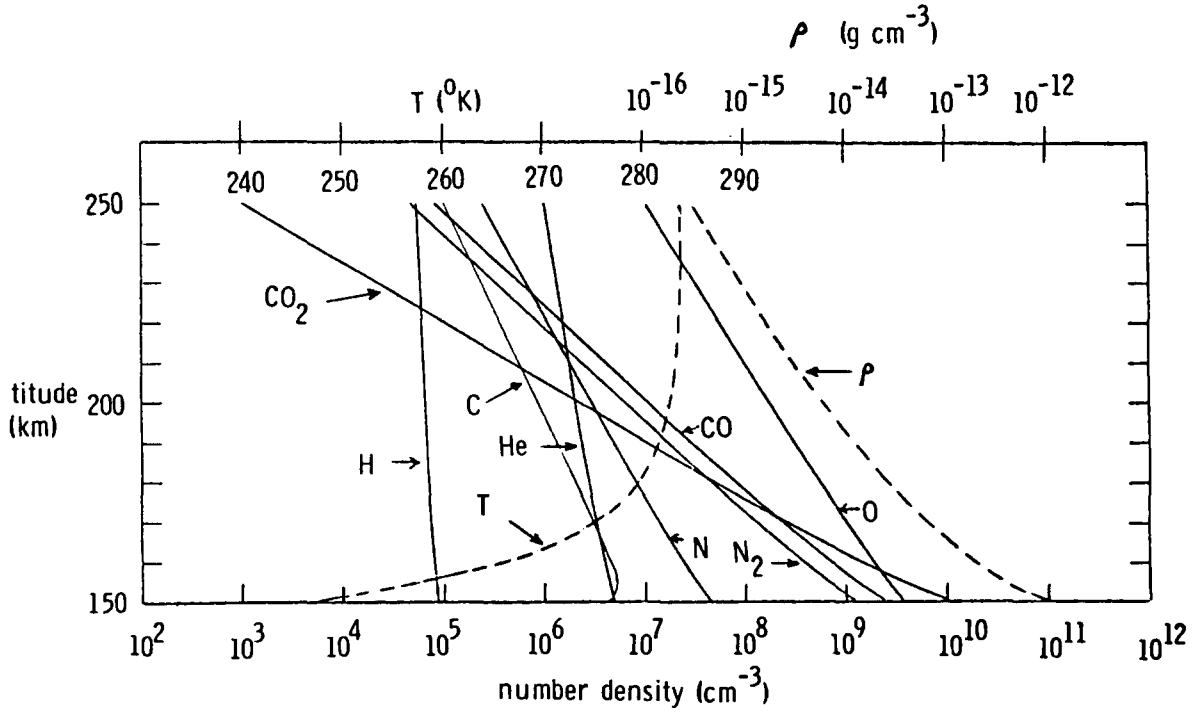

Figure 4-6. Day-Side VIRA Model (150-250 km)

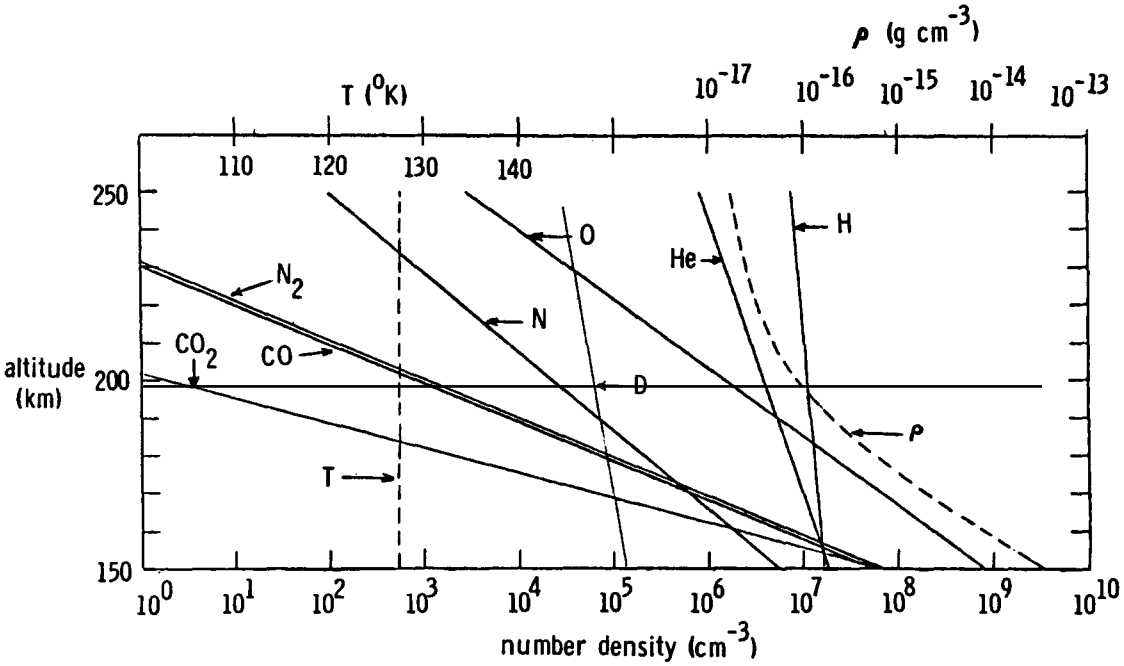

Figure 4-7. Night-Side VIRA Model (150-250 km)

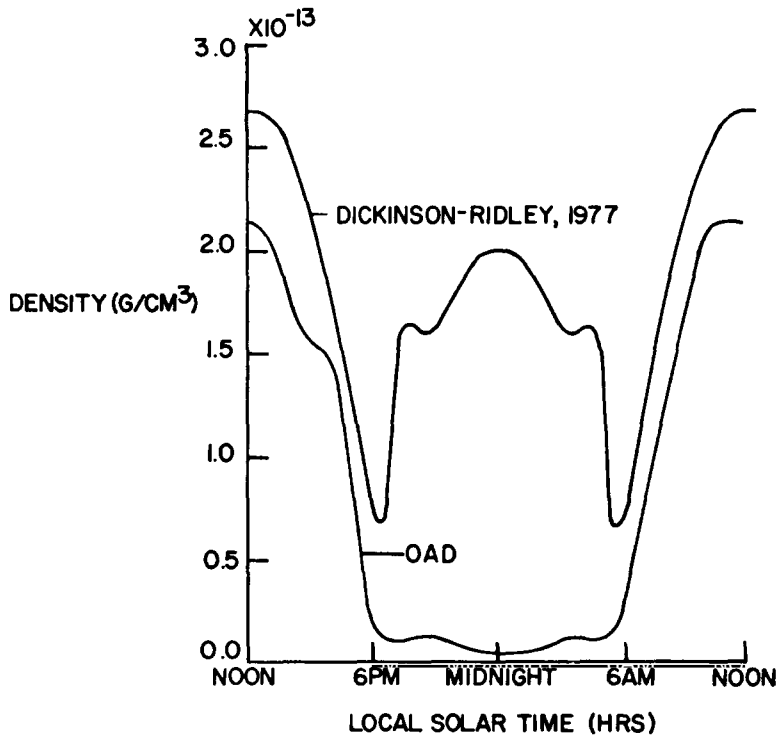

Figure 4-8. Comparison Between Pre-Pioneer Venus Model of Diurnal Variation of Atmospheric Density at 160 km (Dickinson and Ridley, 1977) and the Diurnal Variation Based on Pioneer Venus OAD Data (Keating et al., 1980)

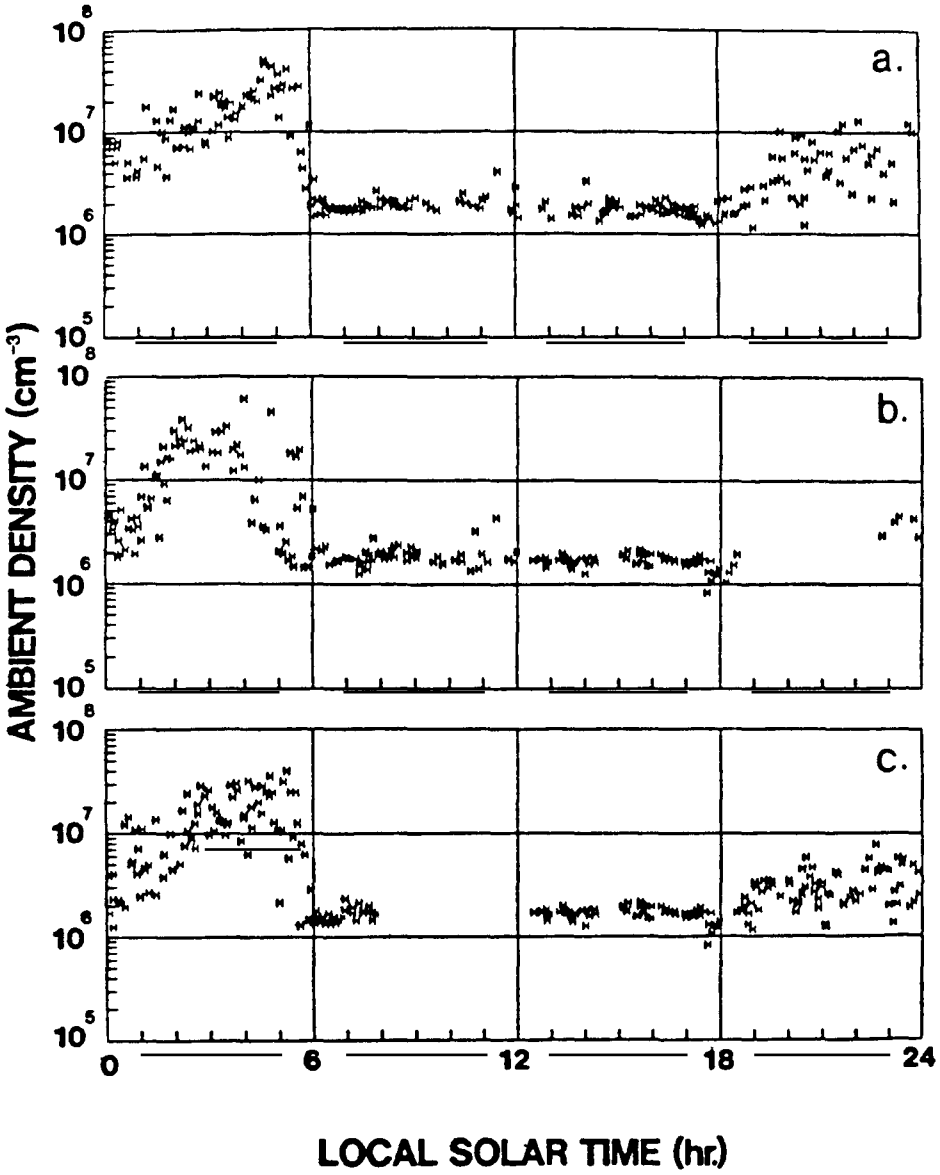

Figure 4-9. Measurements by ONMS of n(He) at 170 km as Functions of Local Solar Time Over Three Diurnal Cycles (von Zahn et al., 1983)

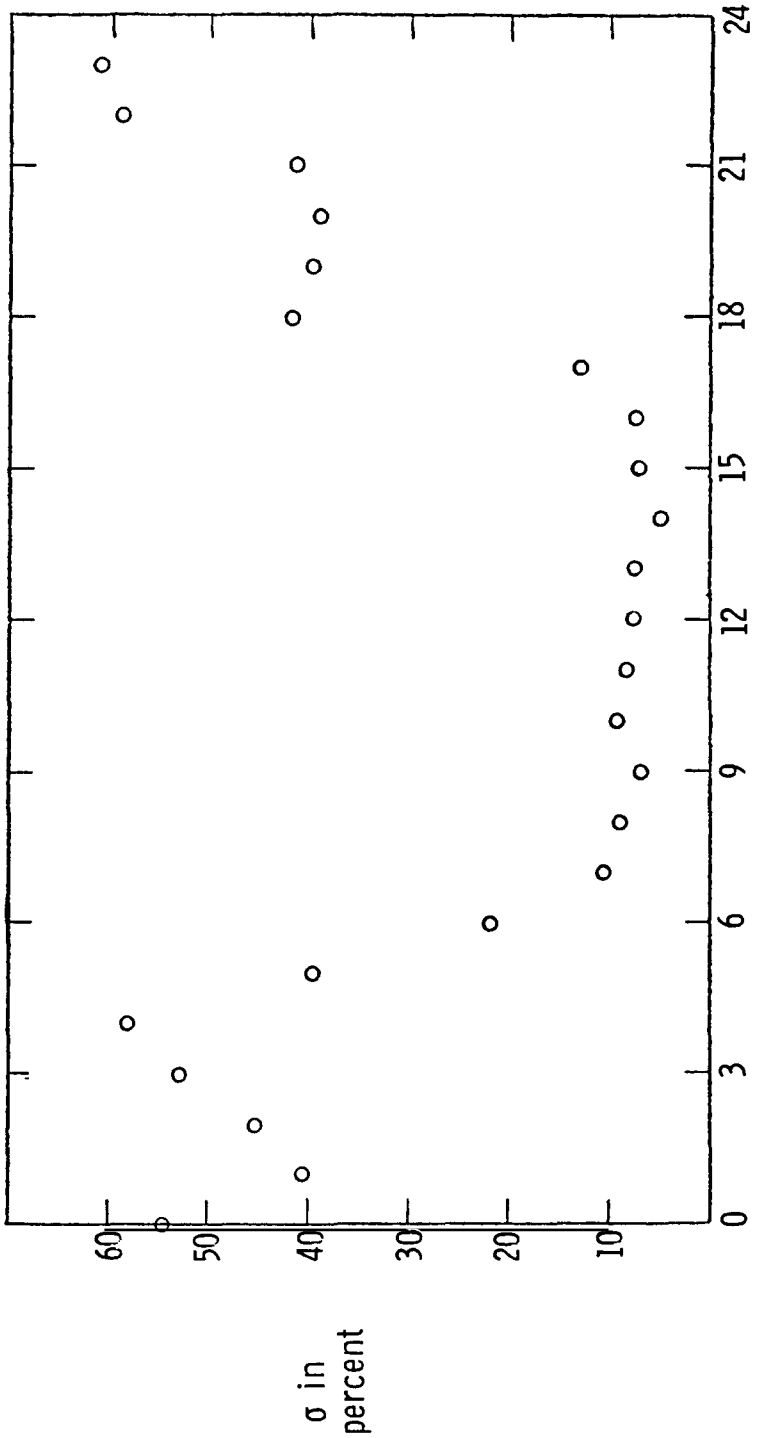

Figure 4-10. Standard Deviation of Daily Values of Atmospheric Density Measured by OAD as a Function of Local Solar Time

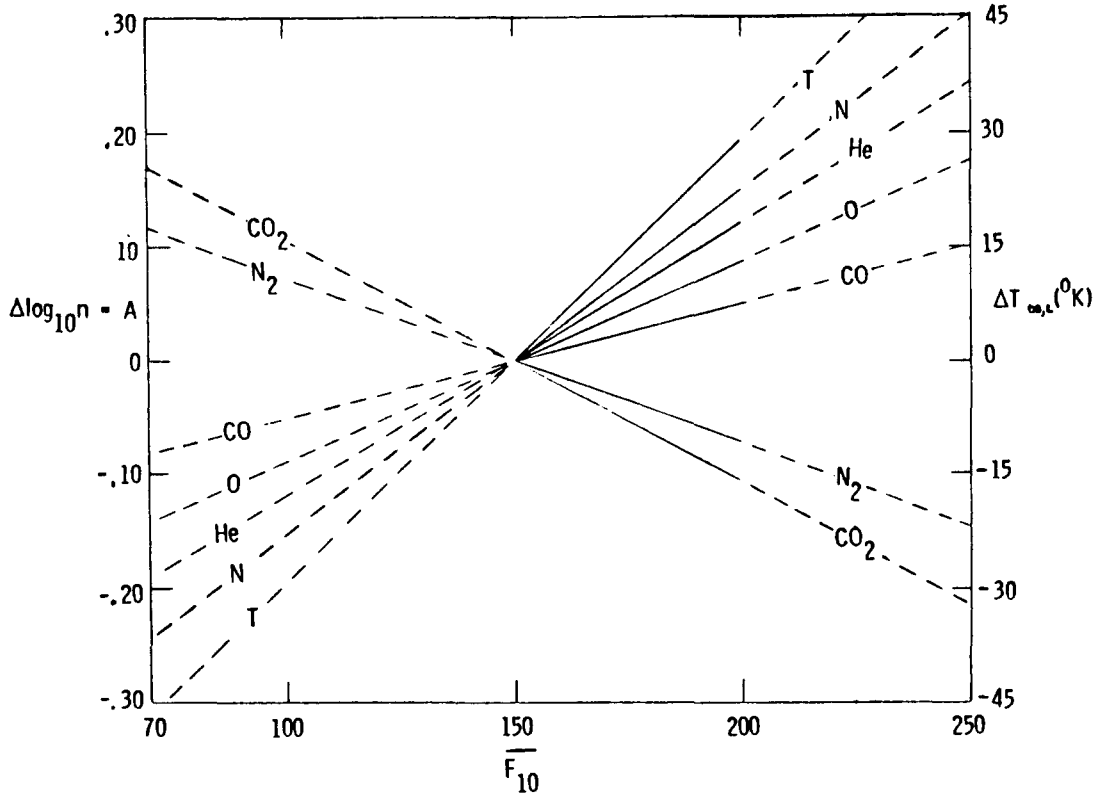

Figure 4-11. Parameters Giving Long-Term Response of Atmosphere to $\bar{F}_{10}$ Index Where A and $\Delta T_{\infty,L}$ Are Defined in Equation 9

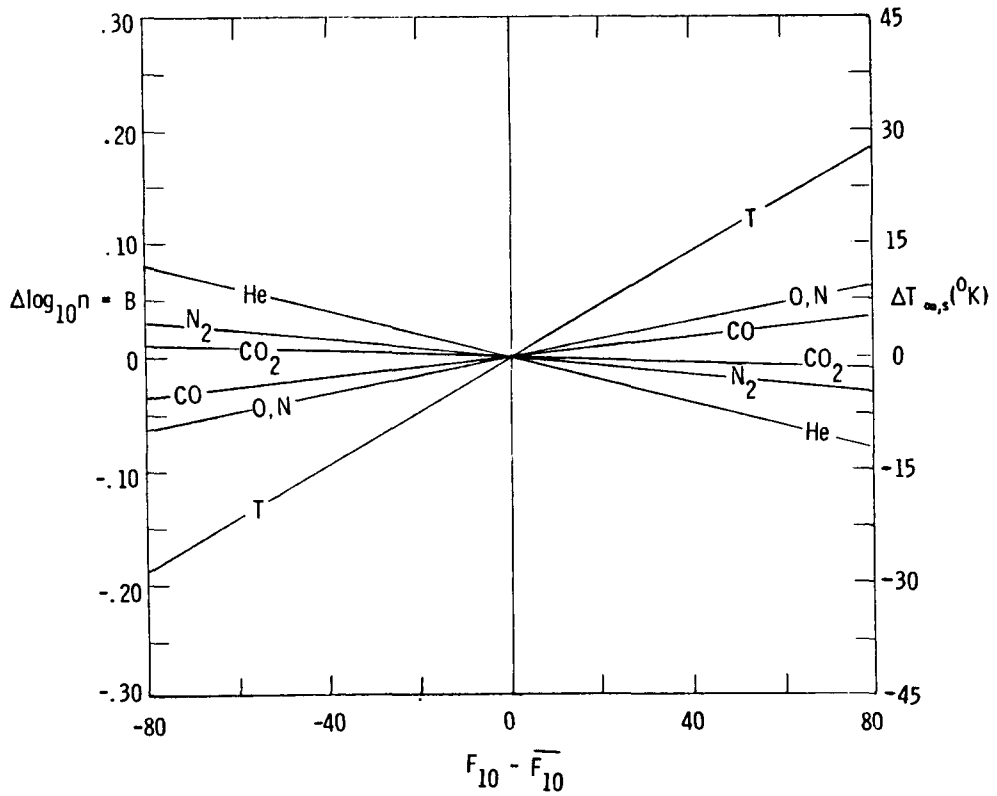

Figure 4-12. Parameters Giving Short-Term Response of Atmosphere to F_{10} Index Variations from $\bar{F}_{10}$ Where B and $\Delta T_{\infty,s}$ Are Defined in Equation 10

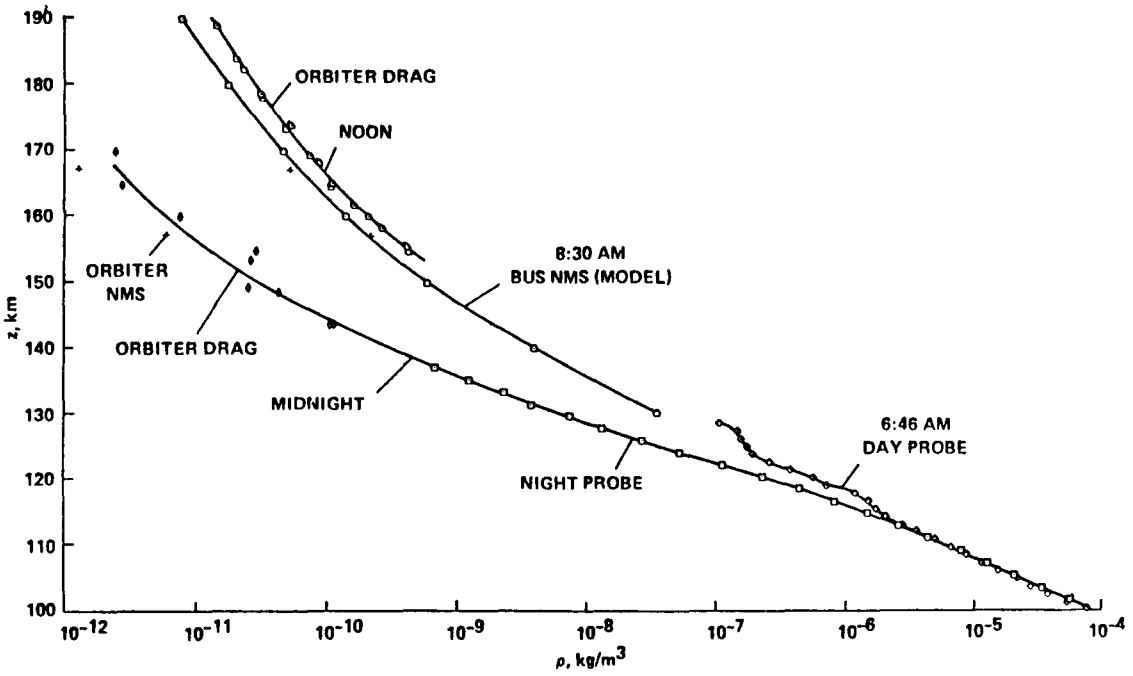

Figure 4-13. Densities in Venus' Upper Atmosphere on the Dayside and Nightside as Measured by a Number of Pioneer Venus Instruments (Seiff, 1983a)

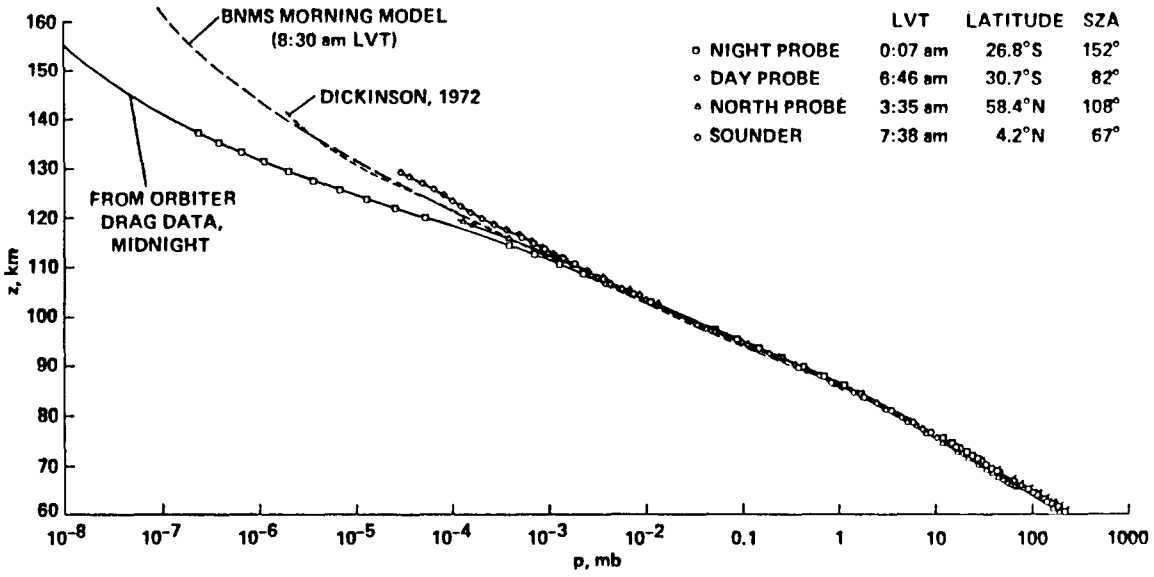

Figure 4-14. Pressures in Venus' Upper Atmosphere on the Dayside and Nightside as Measured by a Number of Pioneer Venus Instruments (Seiff, 1983a)

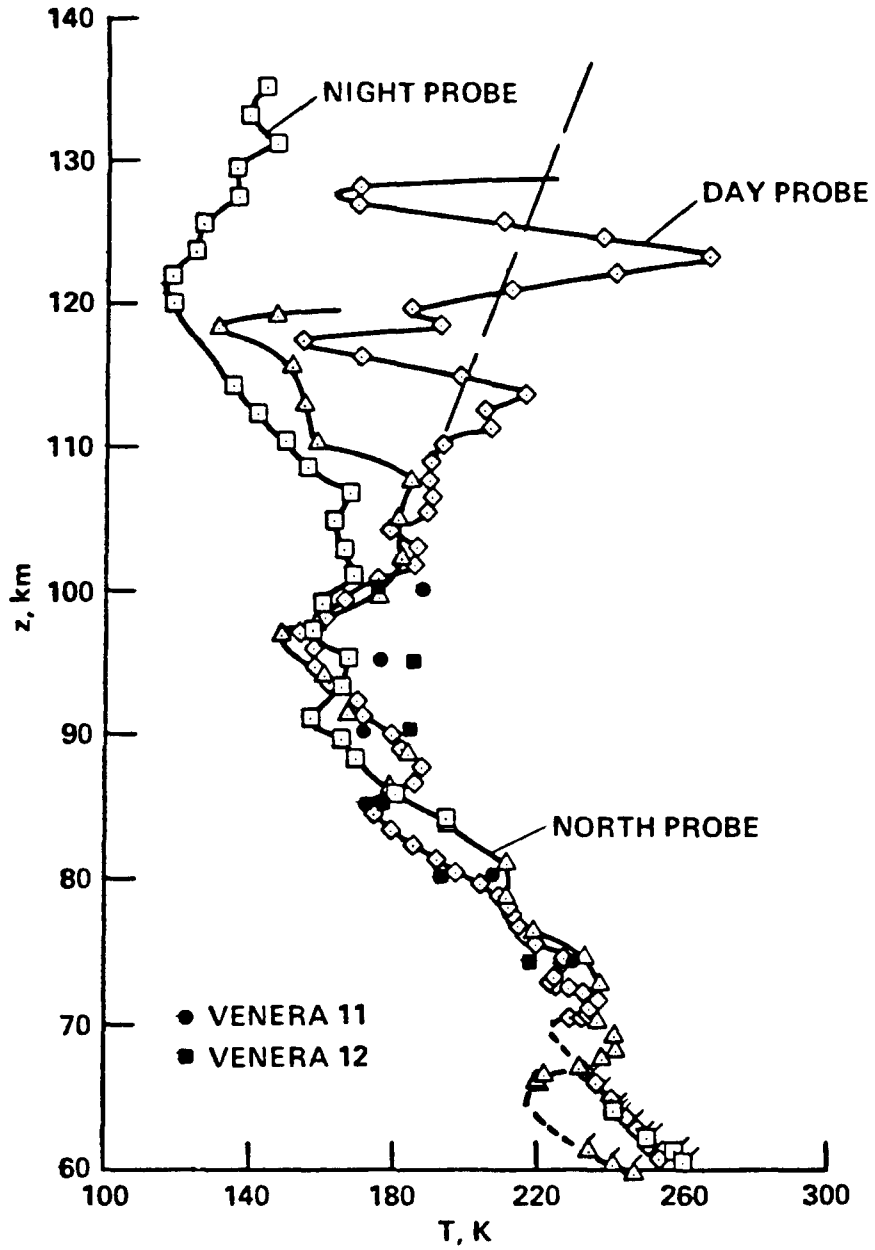

Figure 4-15. Temperatures Above the Clouds Derived from Measurements of Deceleration During Entry of the Three Pioneer Small Probes and Veneras 11 and 12. Flagged symbols show temperatures directly sensed during descent. (Seiff, 1983a)

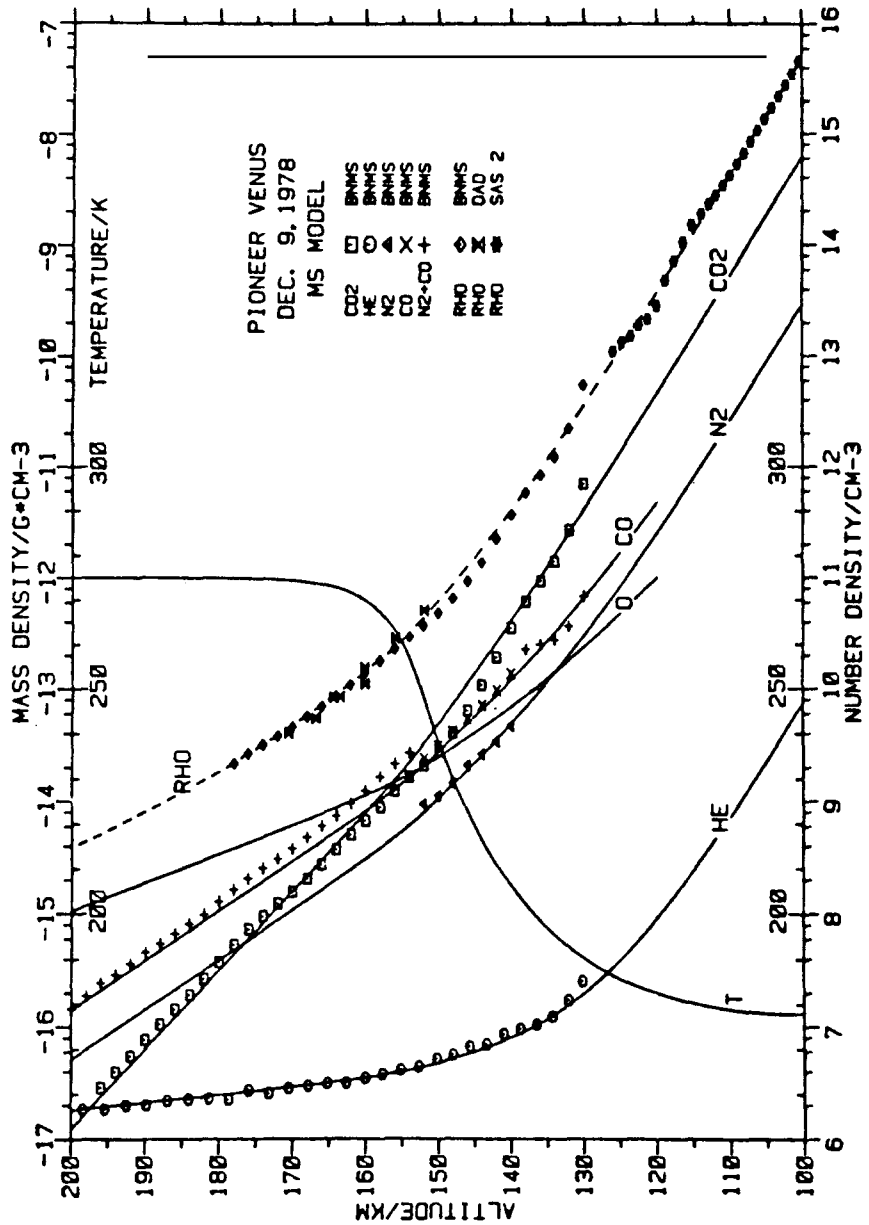

Figure 4-16. Vertical Structure Near 8 AM of n(He), $n(N_2)$, n(CO), $n(N_2 + CO)$ and $n(CO_2)$ Derived from BNMS Data. Also shown is the good agreement with SAS2 accelerometer and OAD drag data (von Zahn et al., 1980).

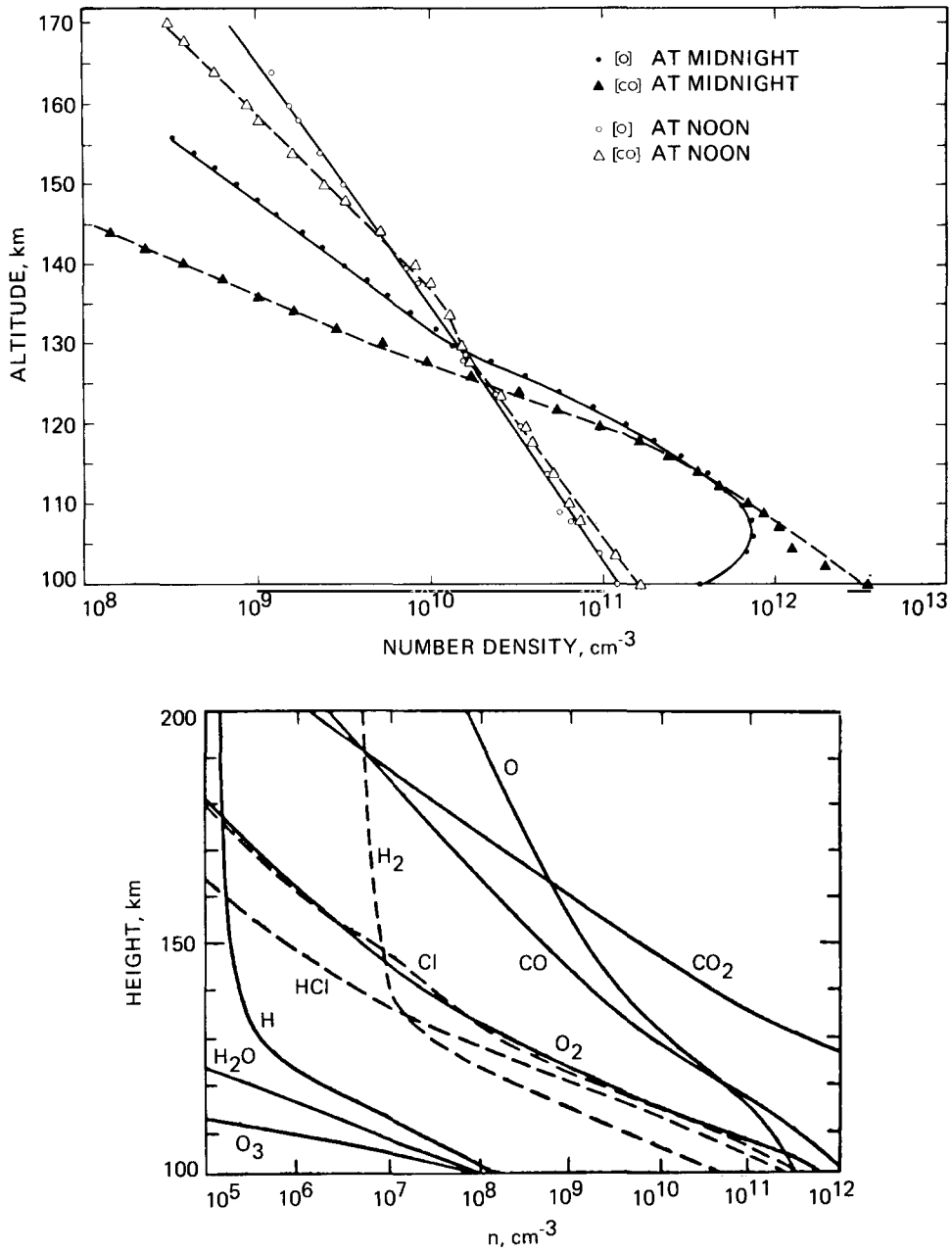

Figure 4-17. Theoretical Models of the Upper Atmosphere
(a) vertical distribution of CO and O for noon and midnight (equator) based on NCAR 2-D model (Bougher, 1986)
(b) theoretical model of the day-side upper atmosphere by Krasnopolsky and Parshev (1981); concentrations indicated by dashed lines have been multiplied by a factor of 1,000

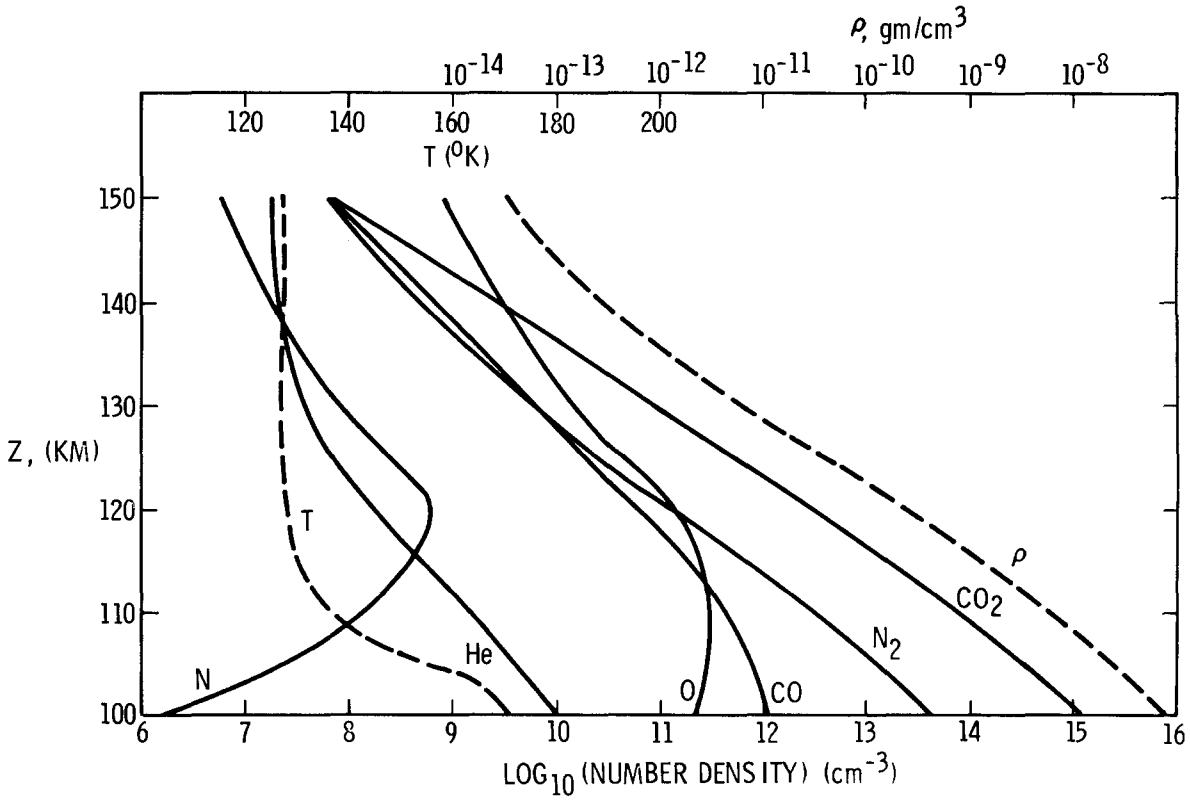

Figure 4-18. Night-Side VIRA Model (100-150 km)

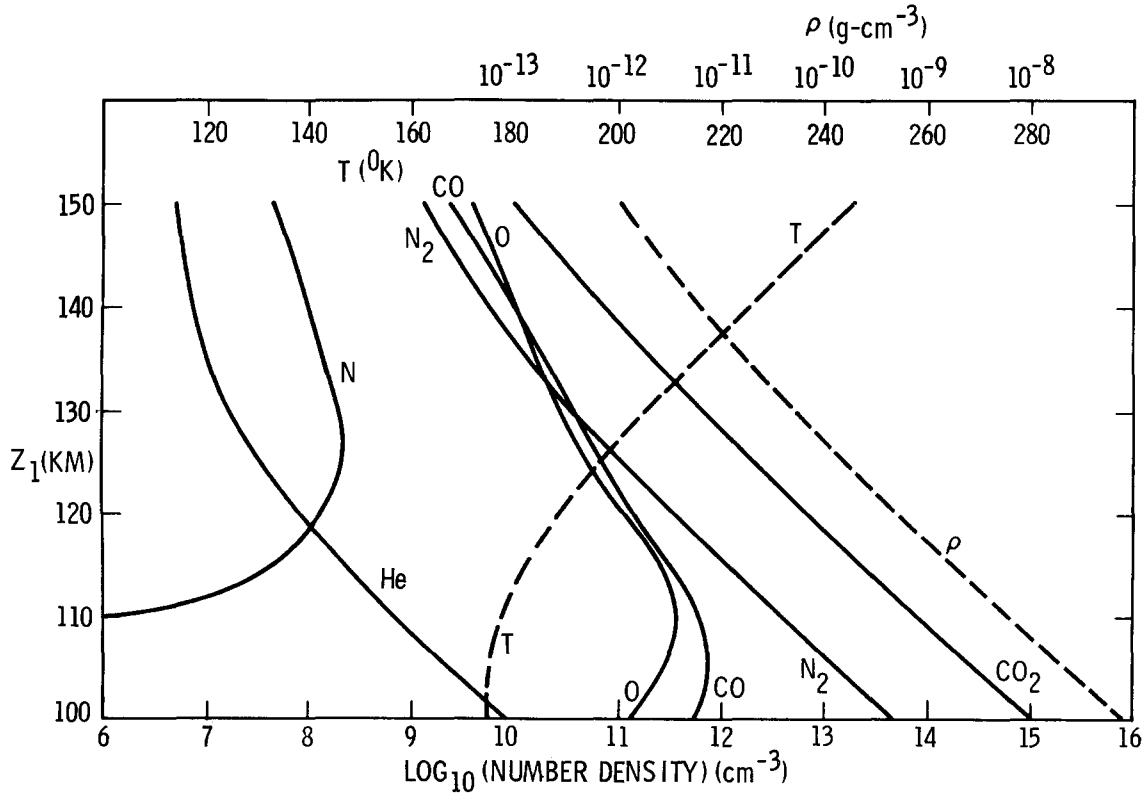

Figure 4-19. Day-Side VIRA Model (100-150 km)

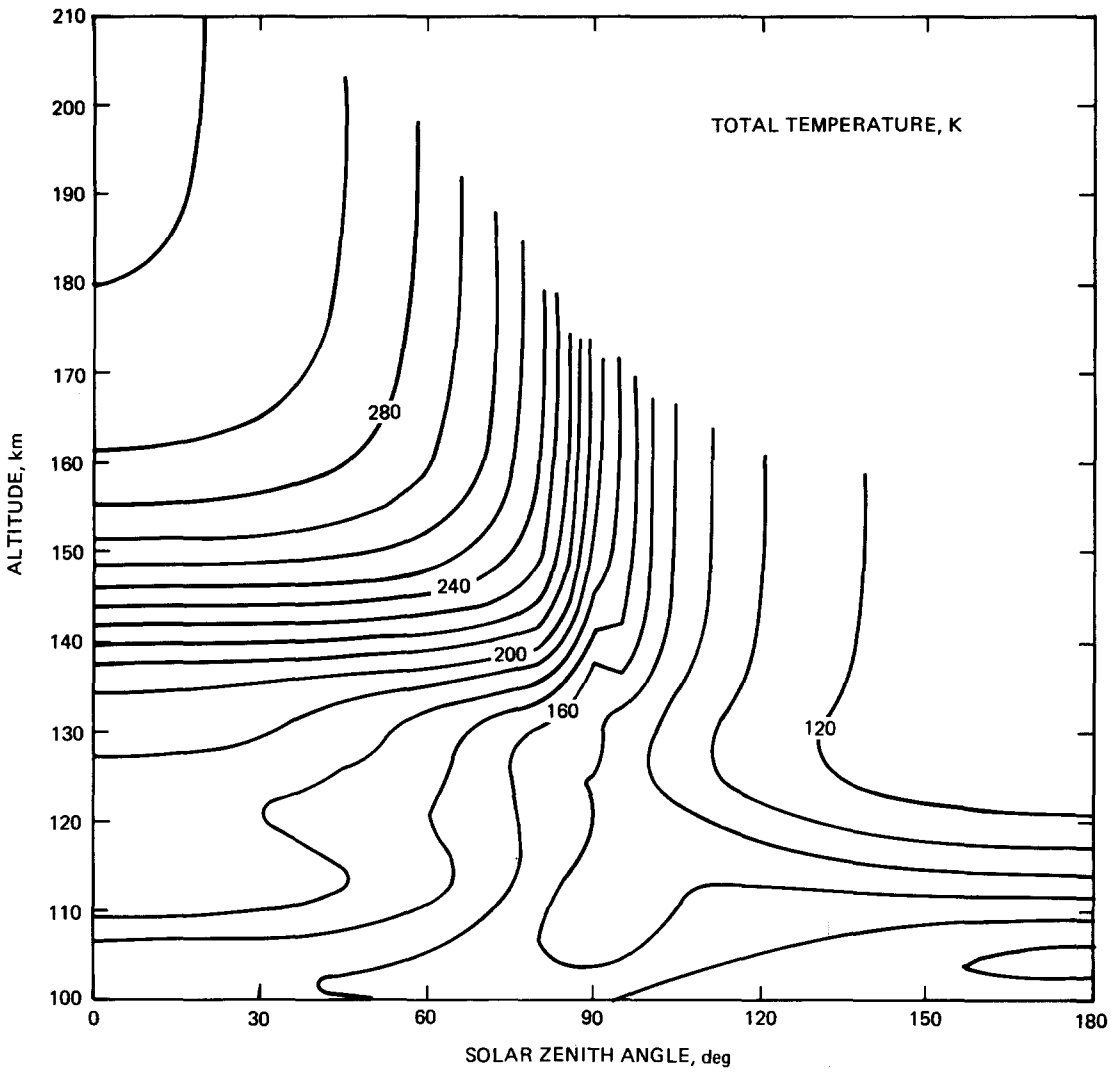

Figure 4-20. NCAR 2-D Model of Total Temperature (K) as a Function of Altitude and Solar Zenith Angle. (Bougher et al., 1986)

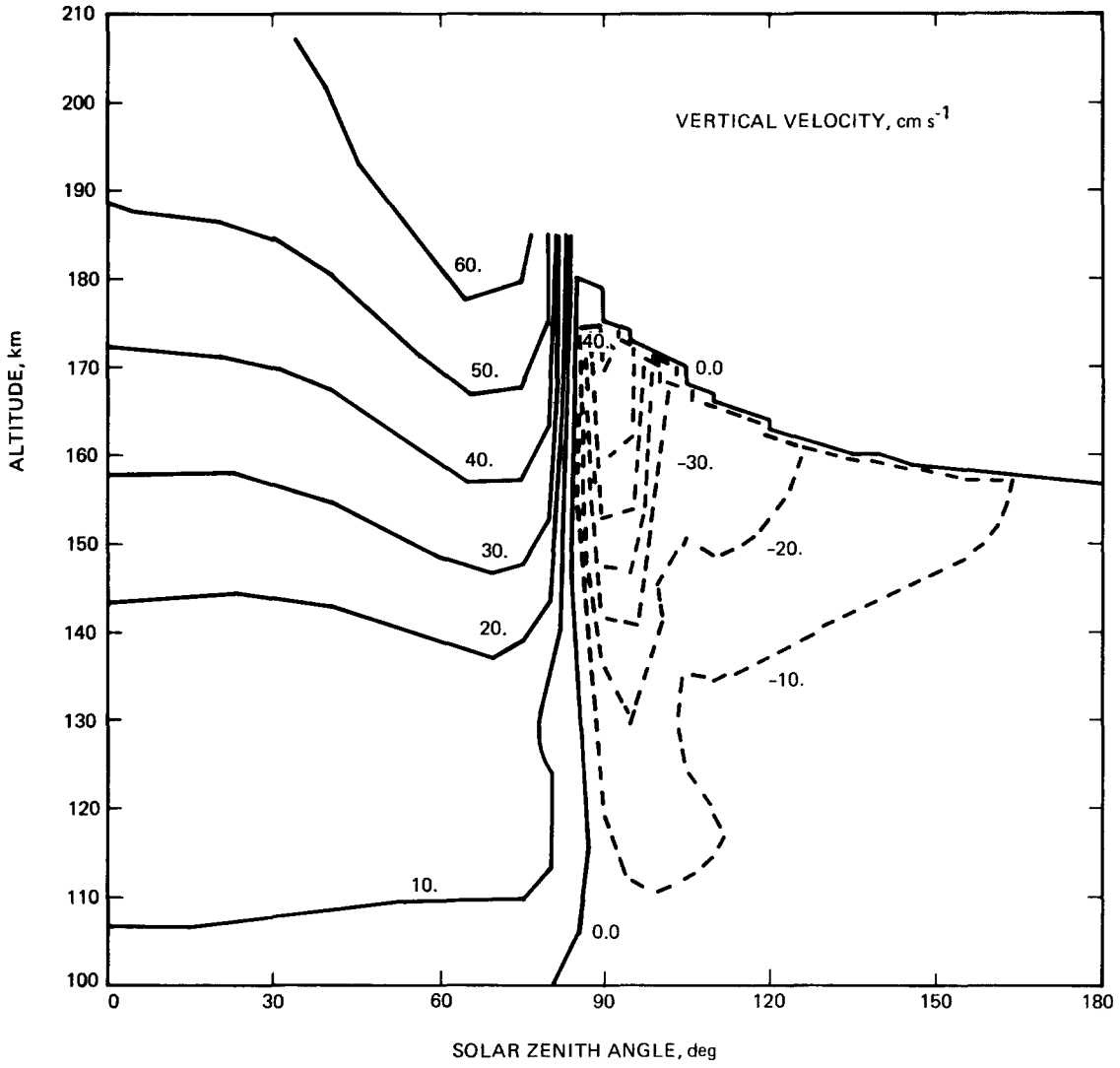

Figure 4-21. NCAR 2-D Model of Vertical Velocity (cm/sec) as a Function of Altitude and Solar Zenith Angle (Bougner et al., 1986)

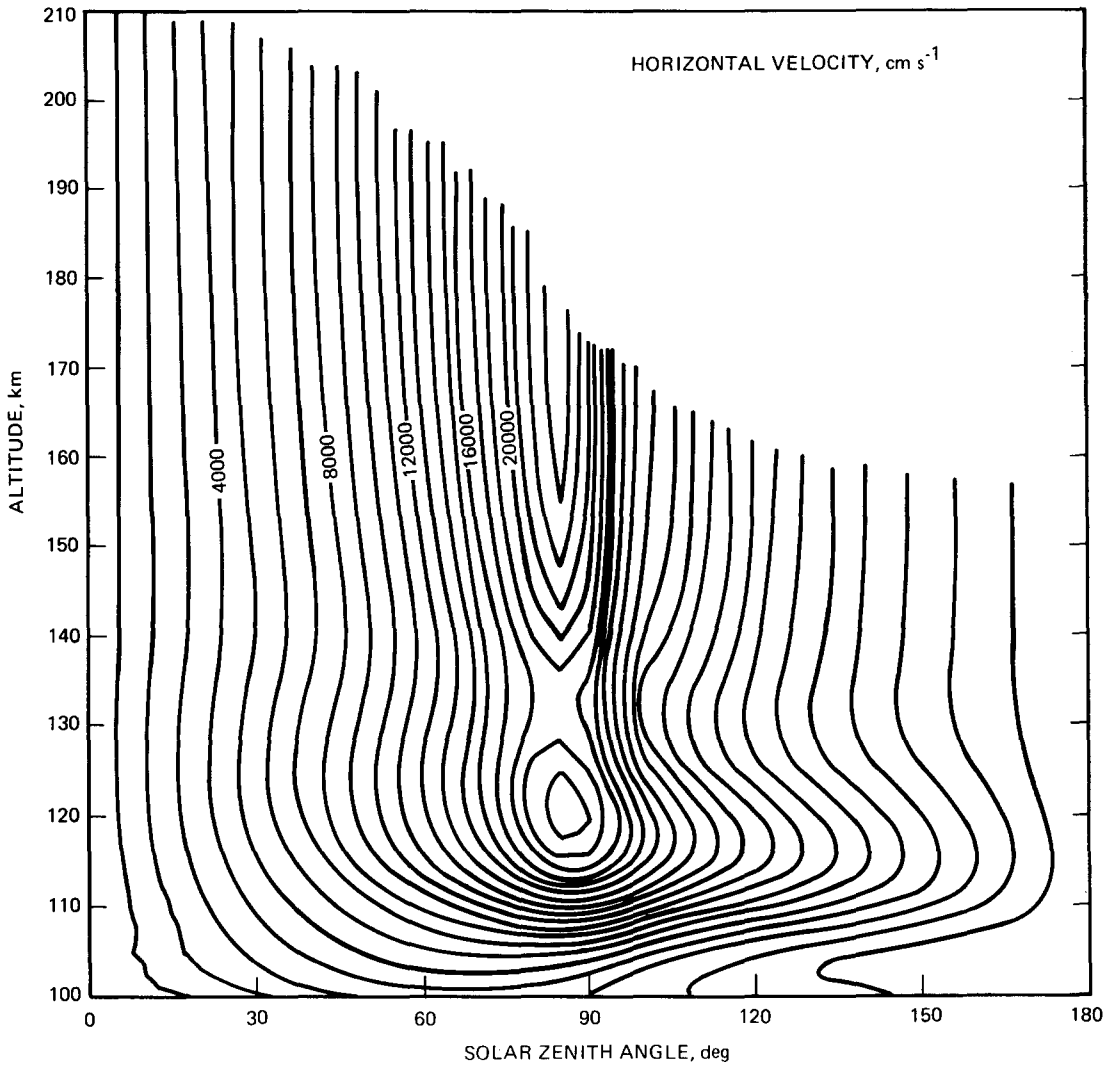

Figure 4-22. NCAR 2-D Model of Horizontal Velocity (cm/sec) as a Function of Altitude and Solar Zenith Angle (Bougher et al., 1986)

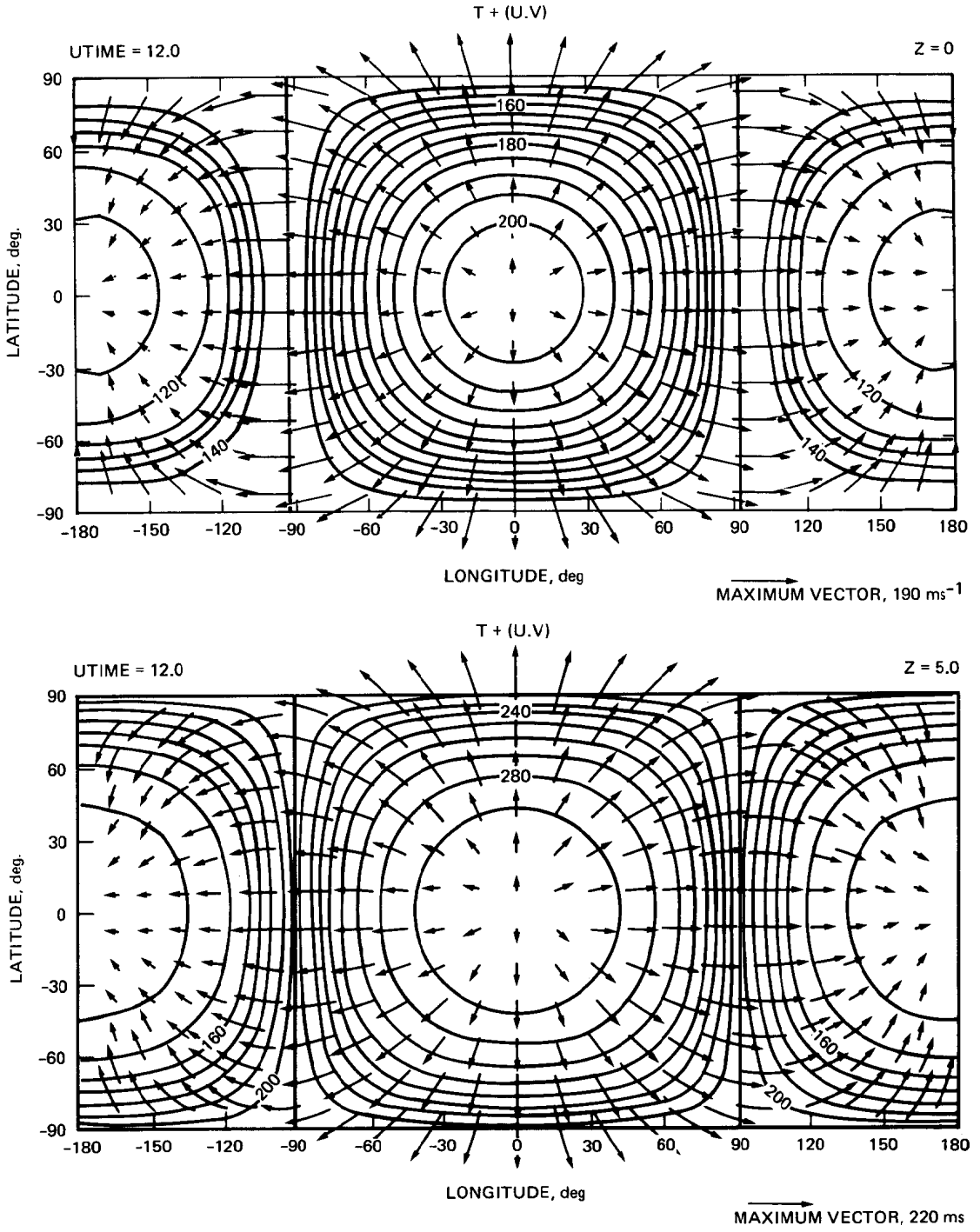

Figure 4-23. NCAR 3-D Model of Horizontal Velocity at Two Pressure Surfaces (defined as function of altitude in Figure 4-24). (Bougher, private communication, 1985b.)

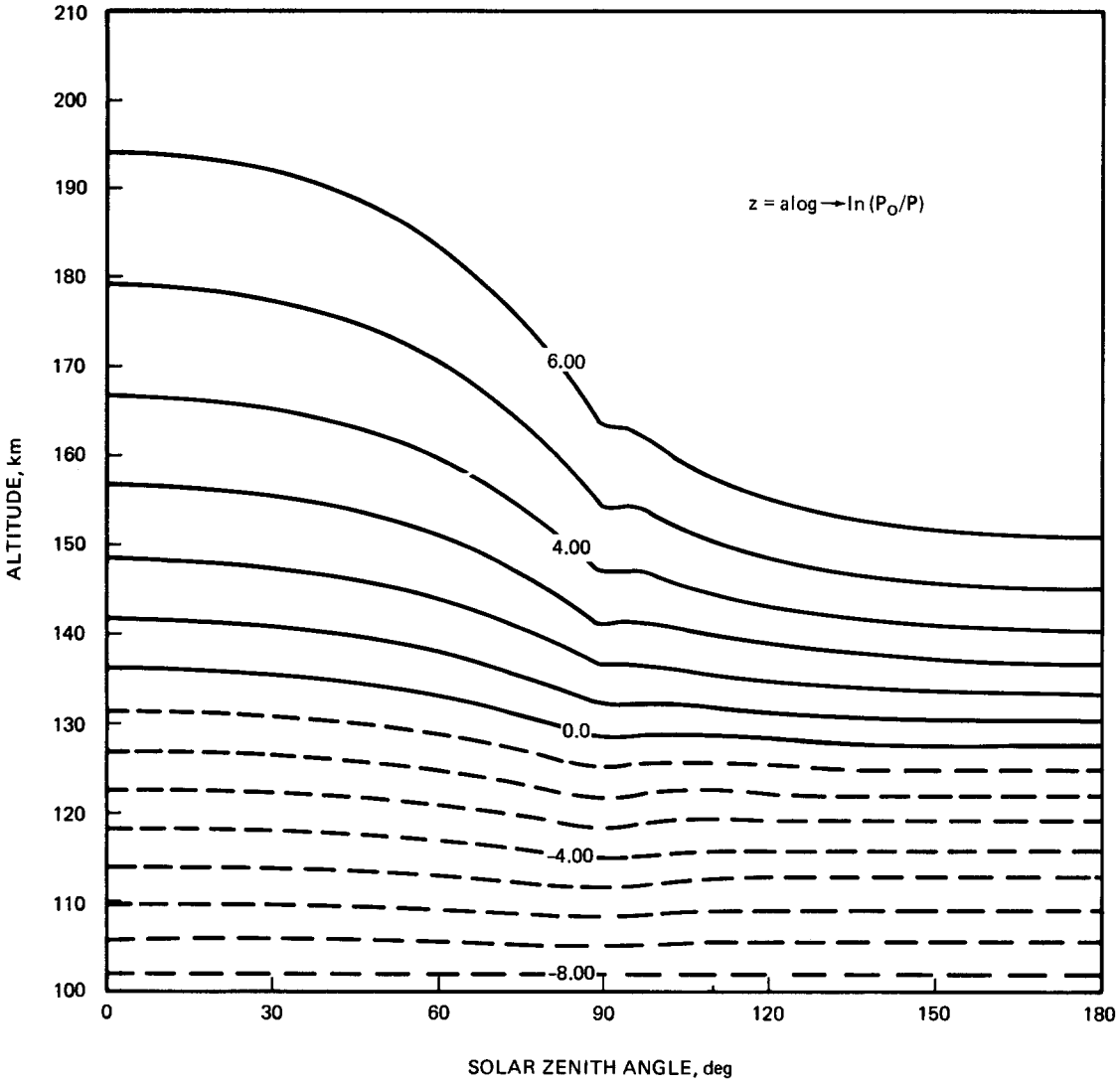

Figure 4-24. Variation of Z, Defined as $\ln(P_O/P)$ where $P_O = 5 \times 10^{-3}$ Microbars and P = Atmospheric Pressure, as a Function of Altitude and Solar Zenith Angle (Bougher et al., 1986)

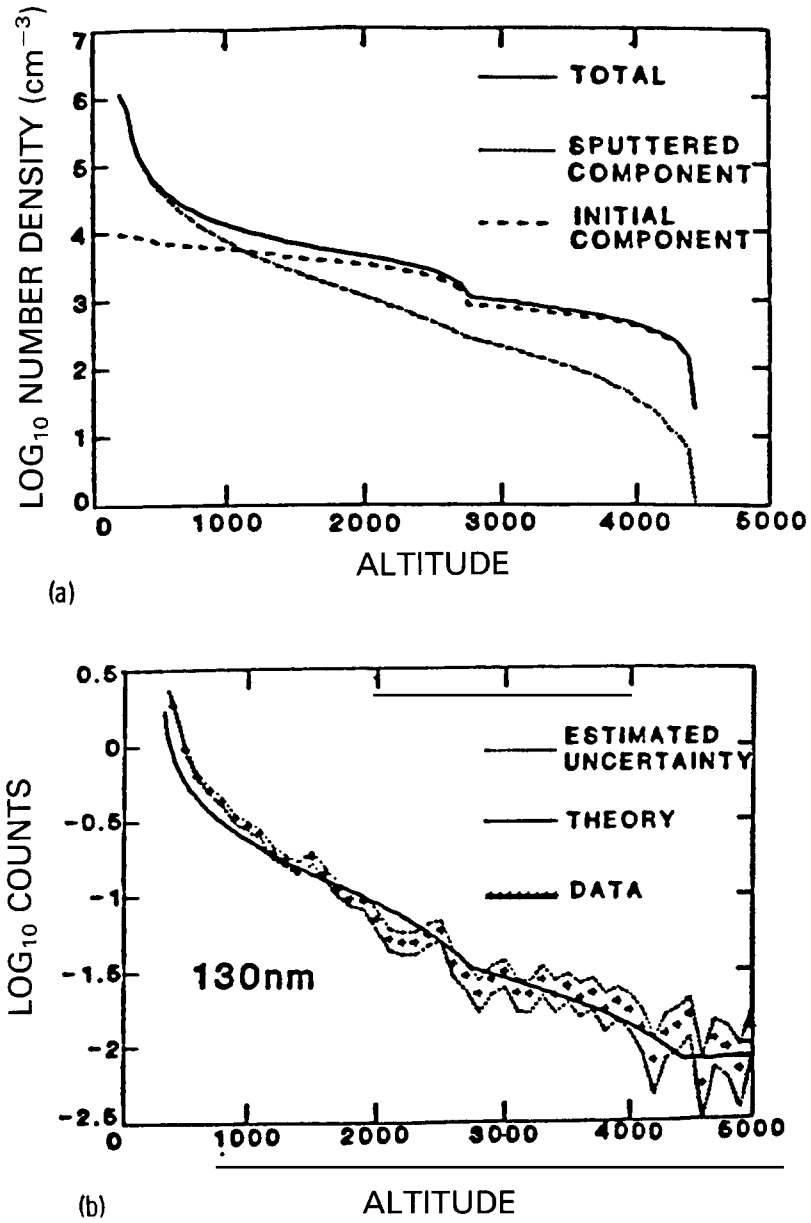

Figure 4-25. Hot Oxygen Atoms in the Venus Exosphere
(a) theoretical distribution of non-thermal oxygen atoms
(b) observations at 130 nm vs. predicted limb signal at 1,304 Å over three orbits of OUVS measurements (Paxton, 1983)

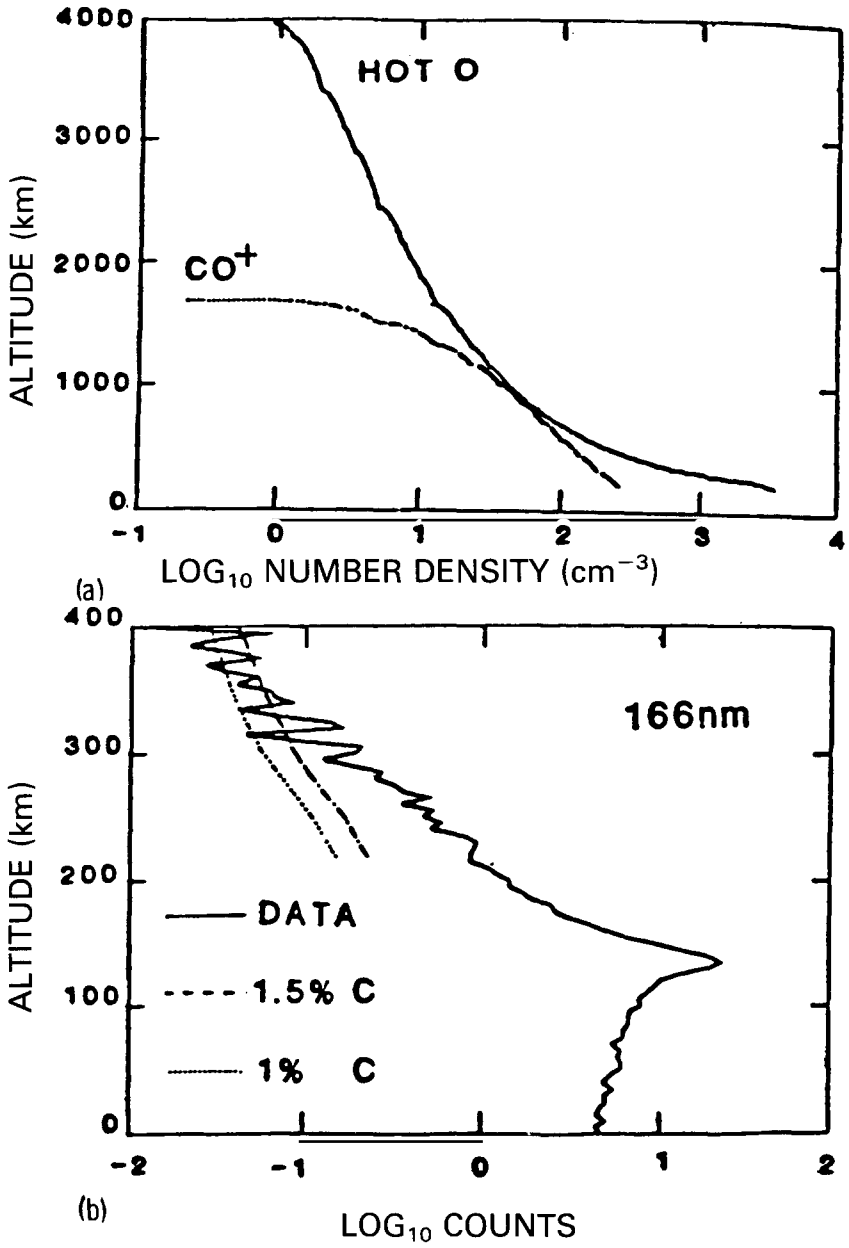

Figure 4-26. Hot Carbon Atoms in the Venus Exosphere
(a) theoretical distribution of non-thermal carbon atoms produced by dissociative recombination of CO^+ and from sputtering of hot oxygen atoms
(b) observations at 166 nm from OUVS limb signal vs. predicted signal for two C to O ratios (Paxton, 1983)

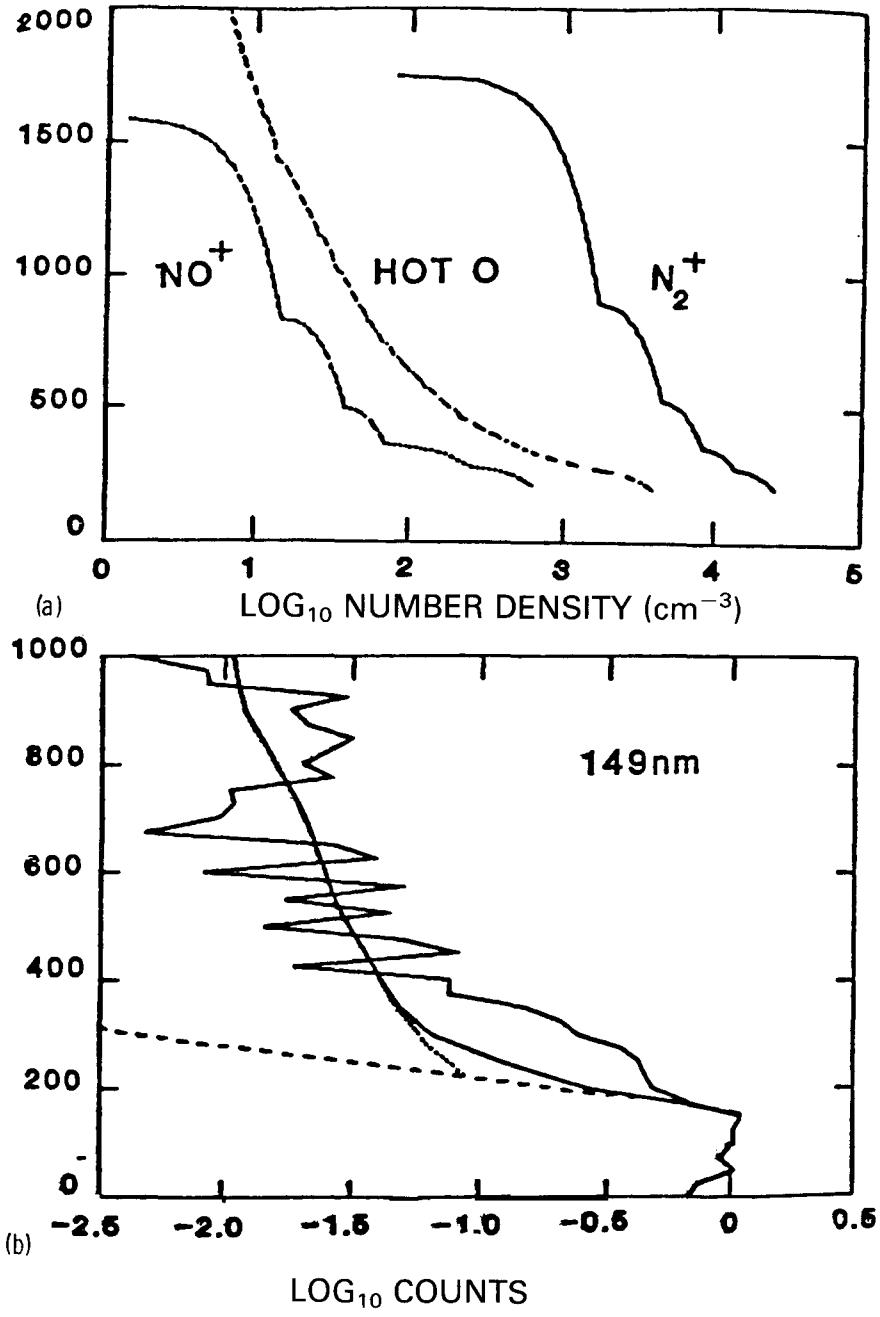

Figure 4-27. Hot Atomic Nitrogen in the Venus Exosphere
(a) theoretical distribution of non-thermal nitrogen atoms produced by three processes
(b) observations of 149 nm from the OUVS limb signal vs. predicted signal at 1,493 Å (Paxton, 1985b)

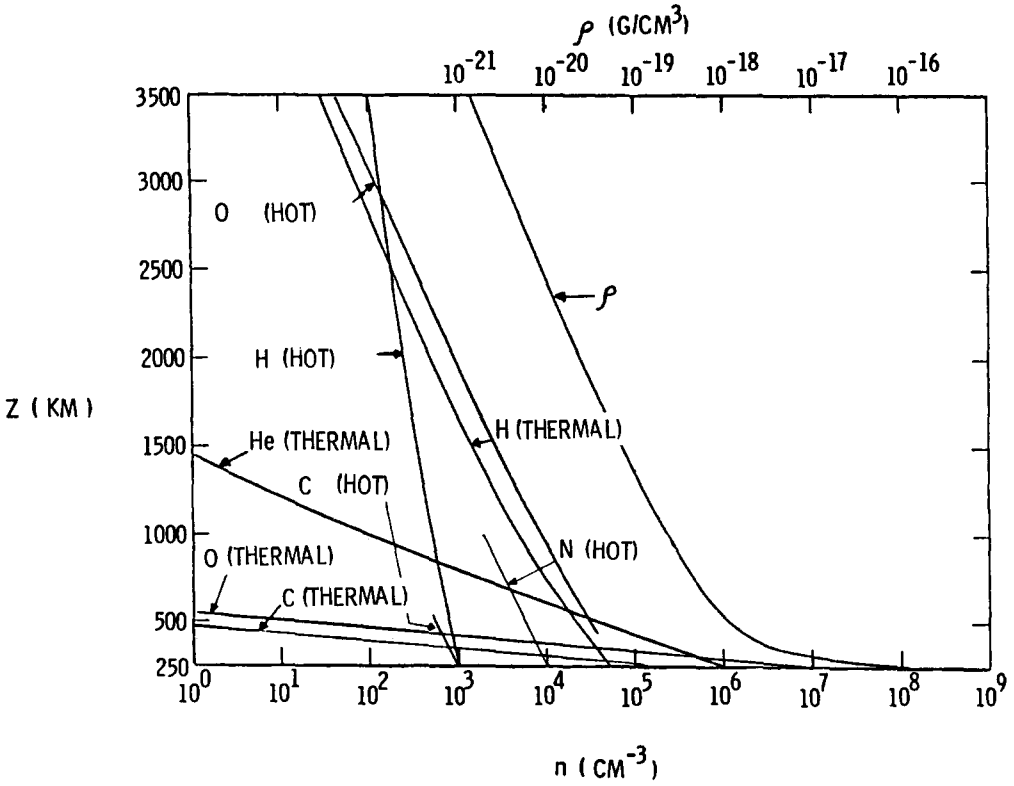

4-28. Day-Side VIRA Model (250-3,500 km)

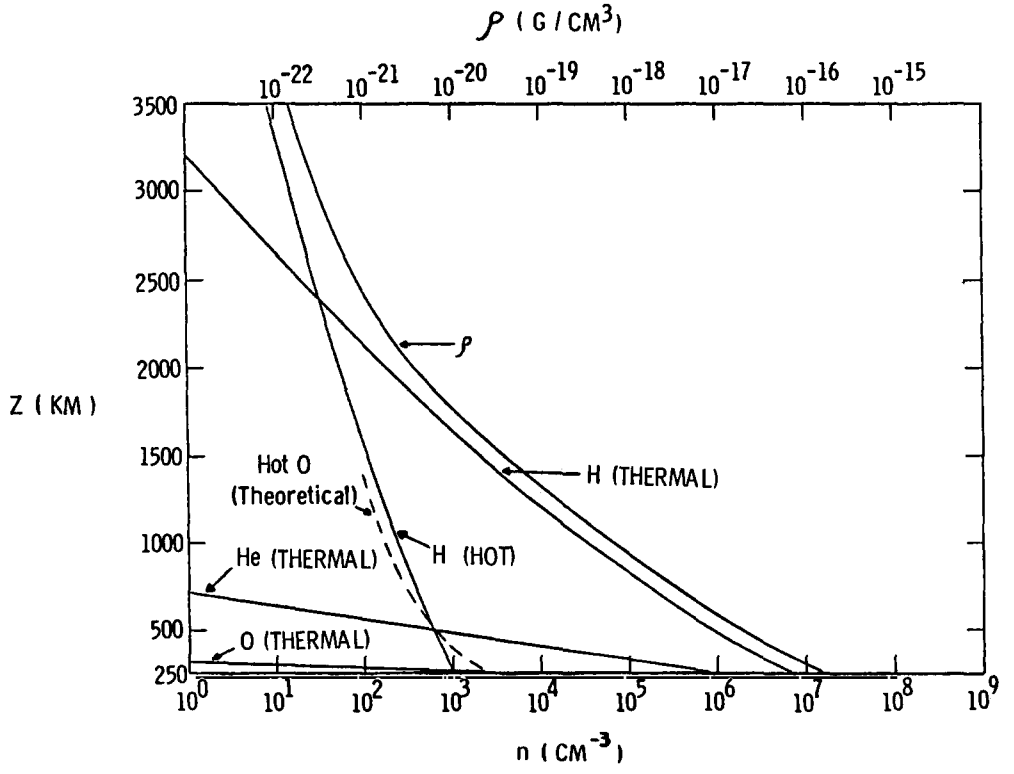

Figure 4-29. Night-Side VIRA Model (250-3,500 km)